Inorganic Controls on Neptunium Mobility in the Subsurface

Peter C. Burns, University of Notre Dame

Final Report

DE-SC0004245

This projected focused on inorganic controls of Np(V) mobility in the subsurface by evaluating co-precipitation of Np(V) into several low-temperature minerals. The minerals were selected so as to provide a variety of cation sites for potential substitution.

A major effort was initially expended to develop synthesis methods for the low-temperature minerals that provided suitably crystalline materials. We focused on production of single crystals of the target compounds because demonstration of Np(V) incorporation is much more robust for these than for powders. We developed a unique method of diffusing nutrients into a barrier solution that slowed nucleation rates and provided excellent crystals of the target minerals. Subsequently, Np(V) was added to the barrier solutions, and we followed the concentration of Np(V) in the solution through time, as well as conducting detailed analysis of recovered crystals. We also conducted all of these same experiments using U(VI) instead of Np(V), so that we could directly compare the incorporation mechanisms.

We hypothesized at the outset of our study that incorporation of Np(V) neptunyl ions in a crystal structure as a dopant could be rather different than for U(VI) uranyl, due to the different charges and bond strengths of the corresponding actinyl ions.

We analyzed all solutions using ICP-MS and ICP-OES methods. We analyzed the collected crystals (and powders in some cases) using a combination of laser ablation ICP-MS, solution-mode ICP-MS for dissolved crystals, X-ray photoelectron spectroscopy and laser induced breakdown spectroscopy (both at the EMSL laboratory), transmission electron microscopy, X-ray diffraction, and UV-vis spectroscopy. The combination of these techniques provided a wealth of information concerning the update of both Np(V) and U(VI) during the growth of low-temperature minerals from aqueous solutions under ambient conditions.

The results of studies focusing on incorporation of the Np(V) neptunyl ion at monovalent cation sites in several minerals were disappointing because essentially no incorporation was observed. This result is surprising because no charge-balance mechanism is needed for this substitution, but over a series of minerals the substitution did not occur.

The studies of Np(V) neptunyl and U(VI) uranyl incorporation into minerals with divalent cation sites proved to be much more fruitful than those focused on monovalent cation sites. In fact, significant amounts of both Np(V) and U(VI) were successfully doped into several minerals grown at room temperature, and their compositions and properties were thoroughly characterized. The results of these studies demonstrate the different behavior hypothesized for Np(V) neptunyl and U(VI) uranyl, and are the first and only study that compares the incorporation of these two actinyl ions into structures under identical synthetic conditions. Furthermore, the data revealed that both the identity of the cation residing in the target site, and the details of its incorporation environment, are important factors in determining the extent of incorporation of into the mineral. The details of the synthesis and characterization are provided in the attached paper "Incorporation of Np(V) and U(VI) in carbonate and sulfate minerals crystallized from aqueous solution" that is under consideration to be published by GCA.

Three doctoral students worked extensively on this project. Jessica Morrison graduated with her PhD in 2013 and is currently working as a science journalist for Chemical and Engineering News. Ernest Wylie graduated in 2014 and is now a post-doctoral researcher in Brian Powell's group at Clemson University. Enrica Balboni will defend her dissertation on November 21, 2014, and has been offered post-doctoral appointments in another group at Notre Dame, and at Lawrence Livermore National Laboratory in the group of Annie Kersting.

The PI and graduate students have presented results of this work at several conferences, including:

Geochemical aspects of nuclear waste disposal
American Chemical Society

Peter C Burns

This presentation will provide an overview of the geochemical aspects of disposal of nuclear waste. The broad categories of waste, their quantities, and their origins will be reviewed, followed by the desired attributes of a geologic repository. With emphasis on matching the waste form to the geochemical environment, various geochemical and materials processes that may occur in the near-field and far-field will be examined, as well as factors that determine the relative importance of these processes in determining repository performance.

Sunday, August 10, 2014 08:30 AM

Incorporation of neptunium into uranyl minerals and various non-actinide low-temperature minerals
American Chemical Society

Peter C Burns*, Enrica Balboni, Ernest Wylie, Nathan Meredith*

Neptunium-237 is a major concern for the long-term disposal of nuclear waste in a geological repository owing to its 2.14 million year half-life and its solubility in water as the neptunyl ion under oxidizing conditions. We have examined incorporation of Np(V) into a variety of uranyl minerals that may form due to the alteration of nuclear waste in a repository, and find that uptake is dependent on the details of the specific target structure as well as the synthesis conditions. We have also examined incorporation of Np(V) into several carbonate, borate, and sulfate minerals in order to determine the specific uptake mechanisms, including site selectivity and charge-balance mechanisms. In general, we find that uptake is strongly dependent on the details of the available crystallographic sites in the minerals for substitution, as well as the specifics of charge-balance mechanisms. We have compared Np(V) uptake in low-temperature minerals with that of U(VI), and find significant differences in uptake levels under identical experimental conditions.

Monday, August 11, 2014 08:10 AM

Role of geochemistry in nuclear waste management
American Chemical Society

Peter C Burns

This presentation will examine the essential role of geochemistry in various aspects of nuclear waste management in the USA and abroad. Emphasis will include the role of geochemical considerations in

repository design and modeling of nuclear waste repositories, including the importance of matching waste forms to geochemical environments for optimal performance. Recent research in the Energy Frontier Research Center *Materials Science of Actinides* of importance to nuclear waste storage and disposal will be examined.

Tuesday, March 18, 2014 01:35 PM

Comparative study of the Np(V) incorporation behavior of calcite and gypsum
American Chemical Society

***Jessica M Morrison**, Peter C Burns.*

Neptunium-237, a byproduct of nuclear fuel, has been listed as a contaminant of concern by the Department of Energy. As an alpha-emitter with a half-life of 2.14 million years, the behavior of Np-237 in the environment is an important area of actinide study.

The interaction between Np(V) and common minerals is being studied to gauge the impact of co-precipitation on environmental fate. Like uranium, neptunium can be present in multiple oxidation states. Np(V) is of specific environmental concern because it occurs under oxidizing conditions and is soluble in water.

We compare the potential for calcite and gypsum to incorporate actinide contaminants--U(VI) and Np(V). The minerals share calcium as a common cation. Its presence in different coordinations allows us to investigate incorporation further based on steric constraints.

Lessons learned from exploratory studies, synthesis technique for growing calcite and gypsum in aqueous solution, and recent results from ICP-MS will be discussed.

Tuesday, August 21, 2012 02:10 PM

Incorporation of neptunium in minerals
American Chemical Society

Peter C Burns

Neptunium-237, with a half-life of 2.14 million years, is a significant potential contributor to the long-term radiation dose associated with a geological repository for nuclear materials, and is a subsurface contaminant of concern. In an oxidizing environment Np(V) dominates over the other oxidation states, and is soluble in aqueous systems. The Np(V) cation forms a linear dioxo cation that is geometrically similar to the U(VI) uranyl ion. However, the different charges of these two actinyl ions result in different structural chemistries. We have examined incorporation of Np(V) into the crystal structures of a variety of U(VI) minerals that may form where used nuclear fuel is altered in a repository.

Incorporation of Np(V) can be considerable but structural constraints of the specific uranyl compound be important. We are also examining incorporation of Np(V) into a variety of synthetic minerals (including calcite, gypsum and borax) to determine the extent to which the neptunyl ion can substitute into different structural sites, and to elucidate charge-balancing mechanisms.

This presentation will review our work concerning Np(V) incorporation into uranyl minerals, and will give results of our current studies of synthetic non-uranium minerals.

Sunday, August 28, 2011 08:40 AM

Incorporation of Np(V) and U(VI) in carbonate and sulfate minerals crystallized from aqueous solution

Enrica Balboni[1], Jessica M. Morrison[1], Zheming Wang[3], Mark H. Engelhard[3], and Peter C. Burns[1,2]*

[1]Department of Civil and Environmental Engineering and Earth Sciences, University of Notre Dame, Notre Dame, Indiana 46556

[2]Department of Chemistry and Biochemistry, University of Notre Dame, Notre Dame, Indiana 46556

[3]Pacific Northwest National Laboratory, MSIN K8-96 P.O. Box 999, Richland, Washington, 99352

*pburns@nd.edu, 301 Stinson-Hall Remick, Notre Dame, Indiana, 46556, Phone Number: 574-631-7852

Abstract. The neptunyl $Np(V)O_2^+$ and uranyl $U(VI)O_2^{2+}$ ions are soluble in groundwater, although their interaction with minerals in the subsurface may impact their mobility. One mechanism for the immobilization of actinyl ions in the subsurface is co-precipitation in low-temperature minerals that form naturally, or that are induced to form as part of a remediation strategy. Important differences in the crystal-chemical behavior of the Np(V) neptunyl and U(VI) uranyl ions suggest their behavior towards incorporation into growing crystals may differ significantly. Using a selection of low-temperature minerals synthesized in aqueous systems under ambient conditions, this study examines the factors that impact the structural incorporation of the Np(V) neptunyl and U(VI) uranyl ions in carbonate and sulfate minerals.

Calcite ($CaCO_3$), aragonite ($CaCO_3$), gypsum ($CaSO_4.2H_2O$), strontianite ($SrCO_3$), cerussite ($PbCO_3$), celestine ($SrSO_4$), and anglesite ($PbSO_4$) were synthesized from aqueous solutions containing either 400 to 1000 ppm of U(VI) or Np(V) relative to the divalent cation present in the system. The synthetic products were investigated by inductively coupled plasma mass spectrometry, luminescence and time resolved luminescence spectroscopy, X-ray photoelectron spectroscopy, and transmission electron microscopy. Amongst the carbonate minerals, calcite significantly favors Np(V) incorporation over U(VI). U(VI) and Np(V) are incorporated in aragonite and strontianite in similar amounts, whereas cerrusite did not incorporate either U(VI) or Np(V) under the synthesis conditions. The sulfate minerals weakly interact with the actinyl ions, relative to the carbonate minerals. Incorporation of U(VI) and Np(V) in celestine was observed at the level of a few tens of ppm; anglesite and gypsum did not incorporate detectable U(VI) or Np(V). Luminescence spectra of the uranyl incorporated in aragonite and strontianite are consistent with a uranyl unit coordinated by three bidentate CO_3^{2-} groups. The time-resolved spectra of calcite indicate multiple coordination environments about the uranyl unit, with the spectra of the longer-lived components displaying similarities with uranyl-incorporated aragonite. The luminescence spectrum of uranyl-bearing celestine is consistent with a uranyl unit coordinated by monodentate sulfate groups. Anglesite synthesized in the presence of uranyl shows no luminescence, whereas the spectra of gypsum and cerussite suggest uranyl surface adsorption or precipitation of secondary uranyl minerals on the mineral surfaces.

Our findings indicate that geometrical constraints of the Np(V) and U(VI) species in solution, together with the crystallographic steric constraints of the host material, affect

preferential uptake in the mineral structures studied. Calcium and strontium appear to be favorable incorporation sites for both U(VI) and Np(V) in aragonite and strontianite. In calcite, Np(V) incorporation is strongly favored over U(VI), whereas in gypsum incorporation of neither actinyl ion occurs. Substitution of actinyl ions was also not observed for lead, in either the carbonate or sulfate minerals studied.

1. Introduction

Neptunium (Np) is created during the burnup of U-based nuclear fuel in commercial reactors for the generation of electricity, and in plutonium-production reactors operated for military purposes. Long-lived ^{237}Np ($t^{1/2} = 2.14 \times 10^6$ y) has been separated from irradiated fuel to be used in the production of ^{238}Pu, which is used in thermoelectric power sources in spacecraft. ^{237}Np is invariably present in irradiated U-based fuels at concentrations that are burnup-dependent, typically in the range of hundreds of ppm, and the combination of its long half-life and high aqueous solubility when it is oxidized to Np(V) make it a potentially important dose contributor in the performance assessment of a geologic repository (Bruno and Ewing, 2006; Burns and Klingensmith, 2006). The quantity of ^{237}Np in irradiated fuel grows with time after the fuel is removed from the reactor, as it is a decay product of ^{241}Am. Neptunium in unaltered irradiated UO_2 fuel will be tetravalent and in substitution for U(IV) in the fluorite-structure lattice (Finch et al., 1999). However, in oxygenated water Np(V) is the stable oxidation state (Antonio et al., 2001; Forbes et al., 2008). Np(V) may enter the environment though a variety of pathways that include the processing of irradiated fuels to isolate fissile isotopes for weapons production or to close a nuclear fuel cycle (Bruno and Ewing, 2006), by the

alteration of irradiated fuel in a geologic repository (Efurd et al., 1998), and by interaction of water with damaged nuclear fuel subsequent to a reactor core-melt event such as happened at Fukushima, Japan in 2011 (Burns et al., 2012). It is therefore important to understand the range of processes that will impact the transport of Np(V) in the environment.

The coordination and crystal chemistry of the pentavalent and hexavalent actinides is dominated by linear dioxo $(AnO_2)^{+,\,2+}$ actinyl ions. These are coordinated by four, five, or six donor atoms of ligands at the equatorial vertices of square, pentagonal, or hexagonal bipyramidal polyhedra. Whereas our understanding of the environmental transport of U(VI) is built upon studies of its extensive mineralogical diversity (Burns, 2005) and its aqueous geochemistry (Altmaier et al., 2013; Clark et al., 1995; Maher et al., 2013), Np(V) does not occur naturally in any appreciable quantity (Katz et al., 2006), and there is no natural analogue for its environmental chemistry. It may be tempting to base predictions regarding the environmental transport of Np(V) on studies of U(VI), in part because they exhibit similar coordination environments in crystal structures as indicated above, and because it is easier and cheaper to conduct studies with uranium. However, the crystal chemistry of Np(V) has been examined over the past two decades and exhibits major departures from that of U(VI) (Forbes et al., 2008). This is due to the different formal valences of the Np(V) neptunyl and U(VI) uranyl ions, and the strengths of their $An{\equiv}O$ bonds. Specifically, the bonds within the Np(V) neptunyl ion are weaker than those in the U(VI) uranyl ion. This is reflected by the dominance of cation-cation interactions (CCIs) in Np(V) compounds, and the near-absence of these in U(VI) compounds (Burns, 2005; Forbes et al., 2008; Serezhkin et al., 2014). In actinide

chemistry, a CCI designates the situation where an O atom of an actinyl ion coordinates another actinyl ion in the equatorial plane of its corresponding bipyramid (Sullivan et al., 1961). Incorporation of CCIs in Np(V) compounds gives very different modes of structural connectivity, as compared to U(VI), including "cationic nets" (Forbes et al., 2008).

Where Np is an environmental contaminant, it is likely to be present at concentrations that are low enough to preclude the formation of primary Np phases such as Np_2O_5 (Curti, 1999; Kaszuba and Runde, 1999). The aqueous transport of Np(V) in trace amounts may be reduced by co-precipitation in subsurface minerals, or by sorption onto their mineral surfaces, amongst other processes. The details of the interactions of dissolved Np(V) with minerals may strongly influence its mobility.

We have previously shown that synthetic U(VI) hydroxides and silicates can incorporate various amounts of Np(V) (Alessi et al., 2013; Burns, 2005; Burns et al., 2004; Burns and Klingensmith, 2006; Forbes and Burns, 2006). Levels of incorporation are impacted by details of the crystal structure as well as temperature and solution pH under which the compounds form. Here we extend our studies of Np(V) incorporation in minerals in order to probe the solution and crystal-chemical controls on Np(V) incorporation. We have selected low-temperature minerals that can be synthesized at room temperature in an apparatus suitable for including Np(V), and that provide a range of site geometries for potential incorporation. Specifically, the mineral phases considered in this work are calcite ($CaCO_3$), aragonite ($CaCO_3$), strontianite ($SrCO_3$), cerussite ($PbCO_3$), gypsum ($CaSO_4.2H_2O$), celestine ($SrSO_4$) and anglesite ($PbSO_4$).

2. Background

Substitution of Np(V) at a monovalent or divalent cation site in a crystal requires structural accommodation of the NpO_2^+ neptunyl ion that is linear, or nearly so, in the solid state. Np(V)≡O bond lengths are ~1.86 Å and the neptunyl ion is ~ 6.44 Å in overall length, including the radii of the O atoms at either end (Forbes et al., 2008). Within the bond-valence formalism, the Np(V)≡O bonds in the neptunyl ion correspond to ~1.5 valence units (*vu*), resulting in a deficiency of 0.5 *vu* at the O sites. The Np(V) cation in the neptunyl ion has a bond-valence deficiency of ~2.0 *vu*, indicating that it must be coordinated by equatorial ligands to create a stable structure (Forbes et al., 2008).

Studies have shown that natural and synthetic crystals of aragonite and calcite can incorporate U(VI) (Kelly et al., 2006; Reeder et al., 2000; Reeder et al., 2001). Of these, aragonite appears to tolerate higher levels of uranyl incorporation (Reeder et al., 2004). Under alkaline conditions in the presence of air, the $UO_2(CO_3)_3^{4-}$ species dominates U(VI) speciation. Extended X-ray absorption fine structure (EXAFS) spectra demonstrated that the $UO_2(CO_3)_3^{4-}$ species is retained essentially intact upon incorporation into aragonite (Reeder et al., 2000). In contrast, the uranyl coordination in calcite appears to contain CO_3^{2-} groups that are monodentate to the uranyl ion, and therefore the local environment about uranyl in calcite differs from that of aragonite (Reeder et al., 2000). Hypothetically, the uranyl ion is in a more stable local environment when coprecipitated in aragonite than calcite. On the other hand, X-ray absorption spectroscopy studies of a 298 million year old calcite crystal from Italy indicated substitution of U(VI) for Ca^{2+} (Kelly et al. 2006). EXAFS data suggest a coordination

environment about the U(VI) cation consisting of two axial oxygen atoms at 1.867 ± 0.004 Å and four equatorial oxygen atoms at 2.31 ± 0.01 Å. These results could indicate that the U(VI) environment in calcite evolves over long time scales, becoming more calcite-like and more stable for long term sequestration of uranium (Kelly et al., 2006).

Coprecipitation experiments of Np(V) and U(VI) in calcite synthesized from seed crystals indicate that Np(V) neptunyl ions can be incorporated into calcite at a concentration about two orders of magnitude higher than for U(VI) uranyl (Heberling et al., 2008). The study indicates that Np(V) occupies a calcium lattice site, with the two axial oxygen atoms of the neptunyl unit substituting for two carbonate groups of the calcite structure, and four monodentate carbonate units coordinating the Np(V) neptunyl unit in the equatorial plane (Heberling et al., 2008). Incorporation of the neptunyl ion into the Ca^{2+} site in calcite is thought to occur through surface absorption, dissolution and reprecipitation (Heberling et al., 2008; Heberling et al., 2011). A surface complexation model for the sorption of specific lanthanides and actinides into calcite indicates that Np(V) sorption is weaker than that of Sm(III) and Eu(III), Pu(V) sorption to calcite is similar to that of Np(V), and Pu(IV) sorption to calcite is much greater than that of Pu(V) (Zavarin et al., 2005).

Studies of higher valence actinide (V, VI) interactions with gypsum, celestine, anglesite, strontianite and cerussite are limited. A few studies reported different incorporation behaviors of Cm^{3+} and Eu^{3+} in aragonite, calcite, strontianite, celestine and gypsum, as shown by time resolved laser luminescence spectroscopy (TRLFS) (Fernandes et al., 2008). Amongst the Ca-phases investigated, incorporation only of Eu^{3+} and Cm^{3+} occurs in aragonite, whereas calcite shows both incorporation and surface

complexation of Eu^{3+} and Cm^{3+}, and gypsum shows only surface complexation of Eu^{3+} and Cm^{3+} (Fernandes et al., 2008; Schmidt et al., 2009). These differences are interpreted as an indication that incorporation of a dopant in a crystal structure is not only dependent on the nature of the substituted cation, but also on the ability of the dopant ion's electronic structure to adapt to the symmetry of the crystal structure to create sufficient overlap with the surrounding ligand orbitals (Holliday et al., 2012). Experiments performed on isostructural strontianite and celestine showed that both phases incorporate Eu^{3+} and Cm^{3+} with no apparent surface absorption, although the overall amount of dopant incorporated by strontianite is higher than in celestine (Holliday et al., 2012).

The objective of the current study is to grow and characterize single crystals of selected low-temperature minerals containing divalent cations in the presence of either Np(V) neptunyl or U(VI) uranyl, and to determine the extent of incorporation of these actinides into the crystal structures. We selected a synthetic method that would allow the synthesis of single crystals without the use of seed crystals. Our focus is carbonate and sulfate minerals containing Ca^{2+}, Sr^{2+} or Pb^{2+}. Incorporation of actinyl ions into these structures most likely involves substitution at the divalent cation site, or perhaps interstitial incorporation. Where Np(V) neptunyl ions are involved, there must be a mechanism to balance the charge disparity associated with substitution for a divalent cation.

As discussed in more detail below, the conditions needed for nucleation and growth of sparingly soluble crystals are necessarily dynamic. Chemical analysis of crystals grown in such systems can demonstrate incorporation of actinides, incorporation

mechanisms, and maximum incorporation levels under the specific conditions.

3. Methods

3.1. Preparation of stock solutions of Np(V) and U(VI)

Caution: ^{237}Np and ^{238}U are radioactive and toxic. Experiments described here should only be conducted by qualified personnel in facilities appropriate for safe handling of radionuclides.

High-purity $^{237}NpO_2$ was obtained from the Isotopes Division of Oak Ridge National Laboratory. A laboratory stock solution was created by dissolving 200 mg of NpO_2 in concentrated aqueous HNO_3 in a Teflon-lined Parr reaction vessel at 150°C for 3 days. Once the solution had cooled, a UV-Vis spectrum for a small sample indicated the presence of Np(V) and Np(VI). $NaNO_2$ was added to the solution to reduce Np(VI) to Np(V), and a subsequent UV-Vis spectrum indicated only Np(V). The Np(V) was then precipitated from the solution by adding NaOH, and the precipitate was recovered by centrifugation, washed, dried, and dissolved in 1 M aqueous HCl. A 30 mM Np(V) stock solution was prepared by diluting an aliquot of the prepared solution. A UV-Vis spectrum collected for the remaining solution confirmed Np(V).

A 0.03M U(VI) stock solution was prepared by dissolving purified $UO_2(NO_3)_2.(H_2O)_6$ in 1M HCl. The concentration of the stock solution was confirmed by inductively coupled plasma optical emission spectroscopy (ICP-OES).

3.2. Synthesis

Experiments using ^{237}Np are difficult and costly because of its radioactivity and

toxicity. *It is essential to conduct experiments with suitable containment and small quantities of neptunium in specialized facilities.*

To facilitate characterization and demonstration of incorporation of Np(V), it is important to synthesize single crystals of target phases wherever possible (Burns and Klingensmith, 2006). A variety of methods exist for the synthesis of sparingly soluble minerals at low temperatures, but only those that provide for the slow comingling of nutrients are likely to give single crystals. One of the most effective of these methods is diffusion of nutrients into a silica hydrogel in a U-shaped glass tube opened at both ends for introduction of solutions (Fernandez-Diaz et al., 2006; Franke et al., 1981; McCauley and Roy, 1974). The method works well because solutions containing nutrients diffuse into the gel from both sides, and crystals nucleate where the solutions intermingle. Variables include the solution concentrations and the degree of hydration of the gel. We have previously used this approach to synthesize uranyl phosphate minerals for crystal structure study (Locock and Burns, 2003; Locock et al., 2005). However, introduction of neptunium into such a system is undesirable, as it results in contamination of the gel and challenging sampling of the crystals because it is difficult to separate individual crystals from the gel.

To avoid the abovementioned issues associated with diffusion in gels, we have turned to a method for the synthesis of sparingly soluble crystals that was first reported several decades ago (Fernelius and Detling, 1934). Two (or more) solutions are passively permitted to diffuse into an aqueous barrier solution, such that the saturation level of the targeted mineral is approached slowly. A schematic of the apparatus used here is shown in Figure 1. It consists of a 100 mL Pyrex beaker that contains two 2-mL glass vials.

These two vials are loaded with 1.5 mL of saturated aqueous solutions of different reaction constituents. The remaining volume in each is carefully filled with an aqueous barrier solution. Subsequently, ~ 60 mL of aqueous barrier solution is added to the beaker, being careful to minimally disturb the solutions in the 2-mL vials. The beaker is covered to minimize evaporation. Solutions gradually diffuse out of the 2-mL vials, forming a stratified aqueous system that has been revealed by the addition of dye to the 2-mL vials in one case (Figure SI 1). The targeted phase eventually crystallizes. The performance of the system is adjusted by modifying the pH of the aqueous barrier, and diffusion of the solutions into the aqueous barrier causes a graduate change of the system pH.

Details of the starting conditions in the synthesis apparatus in each case are summarized in Table SI 1. For example, where the target phase was calcite, the two 2-mL vials were loaded with saturated aqueous solutions of $CaCl_2$ and $(NH_4)_2CO_3$ and the aqueous barrier solution was adjusted to pH ~2 by the addition of 1.0 M HCl. Under these conditions, the aqueous barrier solution remains clear throughout nucleation and crystals appear after a few hours.

The quality of isolated crystals of calcite is related to the initial pH of the aqueous barrier solution. Trials involving a starting pH ranging from 2 to 6 indicated that superior crystals form when starting at the lower pH values. During repeated trials starting from a barrier solution pH of 2, the barrier solution pH was monitored using an Orion PerpHect semi-micro pH electrode. The barrier solution pH was measured every thirty minutes in the center of the beaker, near the top of the solution as shown in Figure 2. The pH probe was initially calibrated against standard solutions of pH 4, 7 and 10. Every thirty minutes,

the pH of each standard solution and then the pH of the barrier solutions in beakers 1, 2 and 3 were measured, in that order. The pH probe was recalibrated every 300 minutes.

Incorporation of Np(V) and U(VI) into the target phases was studied by addition of one of these actinides to previously optimized synthesis setups of the target phase in the apparatus. The quantity of each actinide introduced to the aqueous barrier solution was selected on the basis of the quantities of other cations in the system. Specifically, we identified the cation site in the target compound where the actinyl ion is most likely to substitute, and added the actinide to the solution relative to that cation, at the levels of 400 and 1000 ppm (hereafter designated low and high, respectively). For example, in the case of calcite, we expect Np(V) to substitute for Ca in the structure. We therefore added Np(V) to the system so that it accounted for either 400 or 1000 ppm of the total of Ca + Np. The details for each synthesis are reported in the Supplementary Information (Table SI 1).

Subsequent to addition of the actinide stock solution to the aqueous barrier solution in the synthesis apparatus, 1 mL of the barrier solution was collected for elemental characterization, and this was repeated at 2-day intervals. The collected solutions were stored in 2-mL capped centrifuge tubes sealed with Parafilm. The pH of the barrier solution was measured at 2-day intervals. pH data for the mother solutions of each synthetic mineral phase are reported in Figure SI 2.

An additional calcite synthetic experiment was performed with ~ 7500 ppm of Np(V) in the barrier solution, following the method described above (Table SI 1). The synthesis of this sample was done to obtain a specimen with higher neptunium concentration to provide a strong signal for X-ray photoelectron spectroscopy analyses

and to provide information concerning the potential upper bound of neptunium incorporation in calcite.

3.3. Elemental analyses

Inductively coupled plasma mass spectrometry (ICP-MS) was used to analyze solutions, as well as solids ablated using a laser (LA-ICP-MS). Concentrations of ^{238}U and ^{237}Np were measured in medium resolution for solution samples using a high-resolution magnetic sector ELEMENT 2 ICP-MS. Solution samples were diluted into the ppb range for Np or U in double distilled 5% HNO_3 and were analyzed by the external calibration method. A 1 ppb Tl/Bi internal standard was added to each analytical sample, standard, and blank to monitor for instrumental drift and matrix effects. For synthesis that yielded crystals of suitable size (100s of micrometers), 10-20 crystals for each syntheses were selected and ablated by a 213 nm ND-YAG New Wave Research laser ablation system. Because no laser ablation standard is available for Np, the ratios of ^{43}Ca, ^{86}Sr and ^{207}Pb mass counts to the actinide signal (in counts per second) were measured and used to estimate the upper limit of actinide incorporation in the solid, relative to the non-actinide cation.

Uncertainties for the chemical analyses were calculated based on the standard deviation of the measured intensity for ^{238}U, ^{237}Np, ^{209}Bi and ^{205}Tl, where applicable. The uncertainties for Np and U concentrations are propagated combined percentages based on normalization to an internal standard, ^{209}Bi or ^{205}Tl. The average uncertainty for each set of data is as follows: calcite solution, U (3%), Np (7%); calcite solid, U (8%), Np (6%); aragonite solution, U (5%), Np (5%); aragonite solid, U (8%), Np (7%); gypsum solution,

U (3%), Np (3%); gypsum solid analyzed in solution mode U (3%), Np (2%); celestine solution, U (3%), Np (3%); celestine solid, U (8%), Np (7%); anglesite solid, U (BDL), Np (BDL for crystals synthesized in barrier solutions at 400 ppm; 9% for crystals synthesized at 1000 ppm); anglesite solution U (4%), Np (4%), cerussite solution U (4%), Np (4%), strontianite solution U (3%), Np(3%).

3.4. Powder X-ray diffraction

Powder X-ray diffraction data were collected for various samples during the course of synthesis optimization to evaluate the purity of the synthetic product. Data were collected using a Bruker Davinci automated diffractometer at room temperature over the angular range of 5-60° (2θ, CuKα) with a step width of 0.01° and a fixed counting time of 2s/step.

3.5. Luminescence spectroscopy

Luminescence spectroscopic and lifetime measurements were performed using a Cryo Industries RC-152 cryostat at 10 ± 1.0 K. Ten to 60 mg of each high-uranium-doped synthetic mineral were placed in quartz cuvettes with dimensions 2 × 4 × 25 mm that were closed with silicon stoppers. The cuvettes were mounted on the sample holder of the cryostat (CRYO Industries RC152) with liquid helium vaporizing beneath the sample. The sample was excited with a Spectra-Physics ND:YAG laser pumped MOPO-730 laser at 480 nm. The detection window was gated from 0.05 to 5.2 ms. The beam was detected using a thermally cooled Princeton Instrument PIMAX intensified CCD camera. The

luminescence decay curves were constructed by plotting the spectral intensity of a series of time-delayed luminescence spectra as a function of the corresponding delay time.

3.6. X-ray photoelectron spectroscopy (XPS)

The near-surface oxidation state of neptunium was characterized by X-ray photoelectron spectroscopy (XPS) using a Kratos Axis 165/Ultra DLD spectrometer equipped with Al Kα (1486.6 eV) monochromatic X-ray source. High energy resolution spectra were collected from an analysis area of 300 x 700 microns using a pass energy of 80 eV. The Kratos charge neutralizer system was used for all specimens. Selected neptunium-bearing samples were mounted using conductive double-sided tape attached to a Si (100) substrate. To correct for specimen charging the binding energy scale was shifted referencing the C 1s peak energy of 289.5 eV from the carbonate unit (Engelhard and Baer, 1999). A synthetic powder of Np_2O_5 was used as a standard material to determine the biding energy of Np4f $_{5/2}$ and Np4f $_{7/2}$. The oxidation state of the standard material was confirmed by solid state UV-VIS spectroscopy.

3.7. UV-VIS

Powders of aragonite and cerussite containing Np were dissolved in 1M aqueous HCl. UV-VIS spectra were collected to examine the oxidation state of Np in the material. Data were collected using a Jasco V670 spectrophotometer.

3.8. Transmission electron microscopy (TEM) imaging

U- and Np- bearing powders of selected minerals were suspended in ethanol and added drop-wise onto a copper-supported lacy carbon grid. The samples were imaged using a Titan (FEI) microscope at the Notre Dame Imaging Facility. Imaging was done at 200-Kv under scanning electron and z-contrast modes. Energy dispersive spectroscopy analyses (EDS) were performed for selected spots.

4. Results

4.1. Synthesis

The synthesis apparatus utilized here provides for the nucleation of a relatively small number of crystals, and their subsequent growth, in part because the system changes through time. Figure 2 presents the measured pH of the aqueous barrier solution during three trials of calcite crystallization. The synthesis apparatus creates a system of nutrient diffusion through an aqueous barrier that is initially acidic. By starting the process with a high H^+ concentration (pH ~ 2), the initial interaction of Ca^{2+} and CO_3^{2-} is sufficiently inhibited to prevent immediate crystal nucleation. Where the starting pH of the barrier solution is in the range from 3 to 6, formation of polycrystalline material indicates more rapid nucleation.

During the evolution of the syntheses apparatus of calcite, the pH of the barrier solution increases due to the entry of $(NH_4)CO_3$ from the 2-mL vial (Figure 2). In each of the trials conducted, the initial barrier solution pH of ~2 increased gradually to ~2.5 to 3 over 500 to 700 minutes, and then increased to ~7 to 7.5 relatively rapidly. The exact timing of the onset of the increase in barrier solution pH differs in the three trials. This

aspect of the experiment is not expected to be completely reproducible as insertion and removal of the pH probe causes disturbances in a solution that is partially layered. The observation that the pH in each case increases rapidly over tens of minutes, rather than abruptly, is consistent with the system being initially buffered by the HCl in the barrier solution. The buffer is overcome as diffusion of the $(NH_4)CO_3$ salt solution into the barrier solution progresses.

The slow nucleation and growth of crystals in the apparatus is necessary for the development of isolatable single crystals of the target phases. However, the dynamic nature of the system results in crystals nucleating and growing at different times, as the pH and nutrient concentrations change. Furthermore, if actinyl ions are incorporated into the growing phases in any appreciable quantity, their concentration in the aqueous solution will decrease through time, as they are removed via crystallization. Where actinyl ions are incorporated into crystals of the growing phases, a range of incorporation levels is therefore expected, even within zones of the same crystal that represent a sequence of growth through time. It is also important to consider that the aqueous speciation of the actinyl ions changes over the pH range of the experiments.

The pH profiles of the synthesis systems measured for all other carbonate mineral phases studied here follows the pattern exemplified by calcite. The initial pH was in all cases adjusted to ~2 using a 1M HCl solution, and reached a value of less than 7.8 ±0.1 via a similar transition route as the calcite experiment.

The syntheses of the sulfate minerals under acidic conditions were optimized to obtain large single crystals. For anglesite and celestine, optimized conditions were a pH ~2; for gypsum, the pH was ~5. In the sulfate bearing systems, the pH of the barrier

solutions were constant. Examples of the pH profiles for the syntheses of sulfate minerals are reported in Figure SI 2.

The dynamic nature of our synthesis experiments is not entirely unlike the conditions expected where Np(V) is introduced into the environment. For example, an acidic aqueous solution containing recovered Np released into the subsurface will gradually be neutralized by interaction with subsurface constituents, potentially leading to the precipitation of low-temperature minerals that may incorporate Np(V).

Crystals of calcite, aragonite, gypsum, celestine and anglesite were clearly visible in the apparatus on the edges of the small glass vials after two or three days in both high and low uranium/neptunium concentration experiments. Crystals continued to nucleate and grow along the base of the vials and the 100-mL glass beaker. Crystals and fine grained precipitate were recovered from the apparatus once the pH of the barrier solution reached a steady state, and were washed three times with ultrapure water and dried. Crystals of calcite, aragonite, celestine and anglesite ranged from 100 to 500 micrometers in diameter. Individual blade-like gypsum crystals attained lengths of 5 millimeters. The synthesis of strontianite and cerussite yielded only fine-grained crystalline material. In both cases a precipitate forms within 48 hours at the base of the vials and in the 100 mL beaker of the apparatus. Powder X-ray diffraction data confirmed the purity of the synthetic yields (Figure SI 3).

Vaterite, $CaCO_3$, was present as a minor phase in the calcite product, as shown by powder X-ray diffraction (Figure SI 4). Aggregates of vaterite crystals were readily identified under the microscope, and corresponded to ~ 2% of the product. Calcite was present as a minor impurity in the aragonite product, as shown by powder X-ray

diffraction (Figure SI 4). A few calcite crystals with typical rhombohedral habits were readily identified under the microscope and corresponded to less than 5% of the product. The synthesis products of gypsum, celestine and anglesite did not contain detectable impurities.

4.2. ICP-MS solution mode analyses

Analysis of solution samples of both high and low neptunium concentration barrier solutions from experiments for growth of calcite, aragonite and strontianite by ICP-MS revealed a significant decrease in the Np concentration between Day 1 and Day 3, by which time crystals of the corresponding minerals had formed (Figure 3, Figure SI 5). In the case of the uranium experiments involving aragonite and strontianite, there is a significant reduction of the uranium concentration in the barrier solution between Day 1 and Day 3. However, the uranium concentration in the barrier solution during the synthesis of calcite remains nearly constant through Day 7, after crystals have grown (Figure 3). The concentration of uranium and neptunium in the barrier solution of the cerussite experiments indicates an extensive removal of actinides from solution from Day 1 to Day 7. However, the concentration reduction is more gradual than for calcite (Np), aragonite (U/Np) and strontianite (U/Np).

In contrast to the carbonates, most of the added actinides remained in the barrier solutions during crystallizing of the sulfate minerals. Amongst the sulfates, the celestine synthesis barrier solution shows a ~ 6 % reduction of uranium and ~ 16% reduction of neptunium relative to the initial concentration of actinide in the barrier solution (Figure 4, Figure SI 6). The concentrations of both neptunium and uranium in the barrier solutions

during the synthesis of anglesite and gypsum remained essentially constant through time, with slight increases observed that are attributed to slow evaporation of the solutions.

Crystals separated from the aqueous solutions were rinsed three times with deionized water, with this rinse water captured and analyzed by solution mode ICP-MS. Only samples of cerussite and strontianite yielded detectable amounts of actinides back into solution. The strontianite powder yielded 3 - 6% of uranium and 13 - 15% of neptunium back into solution relative to the quantity in the original barrier solution. The cerussite powders released 30 - 40% uranium and 25 - 30% neptunium upon washing, relative to the concentration of the initial barrier solutions. These results may indicate that the high surface area of these powders enhances their dissolution during washing, that the actinides are sorbed to the powder surface, or that the actinides are present as minor soluble phases. The latter is unlikely because the synthesis method, with abundant water, would not have precipitated a soluble phase.

The sulfate minerals collected from barrier solutions containing low and high concentrations of actinides contained indistinguishable actinide concentrations. ICP-MS solution mode analyses of solutions from the low actinide concentrations are reported in Figure SI 5 and Figure SI 6.

4.3. LA-ICP-MS

LA-ICP-MS results for calcite, aragonite, gypsum, celestine and anglesite crystals provide an upper limit for neptunium and uranium incorporation. LA-ICP-MS analyses of single crystals are invaluable for demonstrating actinide incorporation (or the lack thereof) within the target crystal, as depth-dependent data is available (Burns and

Klingensmith, 2006).

Figure 5 provides LA-ICP-MS data from the measurement of masses corresponding to ^{237}Np and ^{43}Ca for a calcite crystal from the high concentration synthesis experiment. The analysis corresponds to the laser ablation crater evident in the Figure inset. The laser beam struck the sample after the instrument collected background counts for 60 seconds, and immediately counts in the 237 and 43 mass windows occurred (Figure 5). The counts in the 237 window, corresponding to neptunium, remain fairly constant during ablation until the end of the data collection, at 120 s, confirming incorporation of neptunium in the bulk of the calcite crystal. If the Np (or U) was concentrated at the mineral surface, the corresponding count rates would rapidly decline as material deeper in the crystal was ablated. The laser ablation data for gypsum exhibits this type of behavior, for which exemplary LA-ICP-MS data is reported in Figure SI 7.

Fluctuations of the count rate during LA-ICP-MS measurements potentially reflect compositional variations and sample ablation-rate variability. To estimate the maximum actinide incorporation level, the counts per second measured for Np (or U) are compared to the counts measured for ^{43}Ca for calcite, aragonite and gypsum, for ^{86}Sr for celestine, and for ^{206}Pb for anglesite. The known concentrations of these isotopes in the minerals permit estimation of the concentration of the actinides.

LA-ICP-MS results for calcite grown from the high concentration solution indicate that ^{237}Np (~1100 ppm) incorporation is as much as an order of magnitude higher than that for ^{238}U (~148 ppm) in calcite grown under identical conditions (Table 1). The maximum of ^{237}Np measured for calcite synthesized from a barrier solution containing ~ 7500 ppm of Np(V) reaches ~ 5400 ppm (Table 1). The maximum concentrations of

^{237}Np and ^{238}U in aragonite crystals synthesized from a barrier solution with 1000 ppm neptunium are ~ 1500 ppm (Table 1). LA-ICP-MS data for celestine indicates a low level of Np and U incorporation (10-50 ppm) and the neptunium concentration in celestine is about double that of uranium (Table 1).

LA-ICP-MS results for gypsum reveal negligible incorporation of either uranium or neptunium in the synthetic crystals (Figure SI 7). LA-ICP-MS data collected for anglesite crystals synthesized from water containing high and low concentrations of uranium indicated that uranium is below the detection limit in all cases. Low levels (~10 ppm average) of neptunium were detected only for crystals of anglesite synthesized from solutions containing high neptunium concentrations (Table 1). The low levels of actinides present in the sulfate minerals are consistent with the high levels that remain in the aqueous barrier solutions (Figure 4).

4.4. Luminescence spectroscopy

The luminescence spectra for uranyl-incorporated calcite (Figure 6a) and aragonite (Figure 7a) are nearly identical to those corresponding to uranyl in these minerals in previous reports (Reeder et al., 2000; Reeder et al., 2001). The calcite signal exponential decay is best modeled with a double exponential function (Figure 6b), indicating the presence of more than one significant luminescence species ($\tau_1 = 193 \pm 18$ μs; $\tau_2 = 32 \pm 8$ μs). To investigate multiple species further, spectra were collected with the gate for collecting emitting photons briefly open after excitation (0.207-0.707 ms), and then additionally gated for collecting photons at longer delay times (0.907-1.907 ms and 2.207-4.207 ms). The spectra so-collected emphasize the shorter-lived component(s) and longer-lived component(s), respectively. The long-gated components of the calcite

spectra display the character of the spectra of uranyl-incorporated aragonite (Figure 6 c, d; Figure 7 b). This confirms the presence of multiple uranium environments in the calcite structure and indicates that the longer-lived species in calcite are similar to those of aragonite (Figure 6 c, d; Figure 7 b).

The luminescence spectra of uranyl incorporated in aragonite and strontianite are similar (Figure 7 a, c). Spectral maxima for aragonite are at 482.1, 502.5, 523.0, 543.8 and 570.8 nm. The strontianite peak maxima are red-shifted with respect to those of aragonite, and are at 485.0, 505.8, 525.4, 548.6 and 577.2 nm. Time-resolved luminescence spectra of aragonite and strontianite show only a small shift at delay up to 4.0 ms, indicating the presence of only one dominant U(VI) luminescence species in both aragonite and strontianite (Figure 7 b, c). The luminescence spectrum of uranyl-incorporated cerussite is red-shifted with respect to the strontianite spectrum, with peak maxima at 491.0, 512.64, 536.12 and 560.1 nm (Figure 7 d, e). The uranyl luminescence spectrum of cerussite differs from those of the calcite, aragonite and strontianite spectra in that it displays well-resolved and better-defined vibronic peaks.

Uranium luminescence emissions recorded for the sulfate minerals are provided in Figure 8. Note that uranyl concentrations in these synthetic crystals are much lower than in the carbonates. Peak maxima for celestine are at 492.4, 513.0, 535.0 and 561.0 nm. These peaks are consistent with uranyl coordinated by monodentate sulfate units, which for $UO_2SO_{4\,(aq)}$ are at 493, 515, 538 and 565 nm (Vercouter et al., 2008). The time-resolved spectrum of celestine shows no shift with delays up to 4.0 ms, indicating the presence of only one dominant luminescence species (Figure 8b). The exponential decay observed for gypsum is better modeled with a double exponential fit, indicating the presence of more

than one significant luminescence species (τ_1 = 549 μs; τ_2 = 217 μs). The presence of multiple uranium environments is confirmed by the time-resolved spectra, with the long-gate component displaying sharp narrow peaks (Figure 8d). Peak maxima for gypsum are at 491.4, 513.0, 537.1 and 563.0 nm. No uranium luminescence was detected for the anglesite sample (Figure SI 8 c).

4.5. Confirmation of neptunium oxidation state

XPS spectra collected for neptunium-bearing carbonate minerals were evaluated by comparing the shifts of the binding energies to standards. Figure 9 displays the Np4f XPS spectra of calcite and strontianite. The presence of two peaks at ~404.5 eV and 414.8 eV in the spectra is due to multiple splitting of electrons with unpaired spins in the atomic shells $Np4f_{7/2}$ and $Np4f_{5/2}$. In the calcite spectrum, the $Np4f_{7/2}$ and $Np4f_{5/2}$ peaks are at 403.2 and 414.8 eV, respectively, and are 403.3 and 415.0 eV in the strontianite spectrum. In Np_2O_5 the binding energies of $Np4f_{7/2}$ and $Np4f_{5/2}$ are 403.3 and 414.9 eV, respectively. All of these are consistent with $Np4f_{7/2}$ values attributed to pentavalent neptunium (Teterin et al., 2010).

XPS analyses of cerussite and aragonite powders were inconclusive. In the spectrum for the cerussite sample, the Pb4d peak overlaps with the $Np4f_{7/2}$ peak, whereas the surface concentration of neptunium in the aragonite sample was below the detection limit. To determine the oxidation state of neptunium in these two samples, ~ 30 mg of powder were dissolved in 500 μL of 1M HCl and UV-Vis spectra of the resulting solutions were collected. The UV-Vis spectra confirm the pentavalent oxidation state of neptunium in both aragonite and cerussite (Figure SI 10).

The amount of neptunium taken up by the sulfate minerals was in all cases too low to allow for a determination of the oxidation state by XPS or UV-Vis.

5. Discussion

5.1. Np(V) and U(VI) aqueous chemistry

Precisely defining the speciation of U(VI) and Np(V) in the aforementioned synthesis experiments is not a trivial task due to the chemically uneven and changing gradients and changing pH that slow diffusion experiments entail. The saturated salt solutions continuously and slowly diffuse into the aqueous barrier media from the 2 mL vials. This process favors a slow increase in the concentration of the major cations and anions in solution, approaching the mineral saturation slowly. However, crystallization of solids (beginning at Day 2 - Day 3) removes cations and anions from solution, and contributes to local compositional gradients. Considering the Np(V) and U(VI) concentration and the pH of the barrier solution, it is however possible to place boundaries on the primary speciation chemistry of the actinides in these systems. The sulfate syntheses are done in acidic or slightly acidic media, with pH ~5-6 for gypsum and pH ~ 2 for the anglesite and celestine syntheses (Figure SI 2). Under these conditions, dominant species are likely to be NpO_2^+ and UO_2^{2+}, with little hydrolyses or carbonate complex formation. If actinide-sulfate complexation occurs, the most likely species are $Np(V)O_2SO_4^-$ and $UO_2SO_{4(aq)}$, with minor $UO_2(SO_4)_2^{2-}$ and $UO_2(SO_3)_3^{4-}$ present, depending on the actinide/sulfate ratio (Altmaier et al., 2013; Hennig et al., 2009; Neuefeind et al., 2004). Considering the low pH and actinide concentration in these experiments, neptunyl- and uranyl- carbonato complexes formed by interaction with atmospheric CO_2 will be

insignificant.

The carbonate syntheses systems reached a pH in the range of 7 to 8 by the time of crystallization. The uranyl triscarbonato complex, $UO_2(CO_3)_3^{4-}$, is likely to dominate in the experimental conditions containing uranium opened to air and in the presence of added carbonate, although other carbonate or mixed hydroxo-carbonato species such as $UO_2CO_{3(aq)}$, $UO_2(CO_3)_3^{5-}$, and $(UO_2)CO_3(OH)_3^-$ may be present as well in lesser abundance (Altmaier et al., 2013; Silva and Nitsche, 1995). For the Np-bearing syntheses, NpO_2^+ and $NpO_2(CO_3)^-$ could be the dominant species in solution, with other aqueous neptunyl polycarbonate species such as $NpO_2(CO_3)_2^{3-}$ possible (Altmaier et al., 2013; Silva and Nitsche, 1995). Precipitation of Np_2O_5 is not unlikely under these experimental conditions, nor was it observed. The formation of Np_2O_5 from aqueous solution is pH and concentration dependent, such that its precipitation near pH 8.5 requires a Np(V) concentration near 10^{-5} M (Runde W., 2000).

5.2. Experimental data

The experimental data reveal remarkable differences regarding the incorporation of Np(V) and U(VI) into carbonate and sulfate minerals grown in aqueous solution under ambient conditions. Overall, the growing carbonate crystals incorporated both actinyl ions at far higher levels than the sulfate minerals. This is not entirely unexpected, as carbonate is a stronger actinide complexing ligand than sulfate, as has been shown by experimental and computational data (Silva and Nitsche, 1995; Vallet et al., 2012). The large differences in incorporation behavior of U(VI) uranyl and Np(V) neptunyl into the same mineral is also a remarkable observation, and is less easy to rationalize.

All of the compounds under study have divalent cation sites as targets for potential actinide incorporation, and the results clearly demonstrate that the size of the cation site is not the primary factor in determining the extent of actinyl incorporation into a specific phase. This finding is in general agreement with earlier conclusions concerning the substitution of $(NpO_2)^+$ for $(UO_2)^{2+}$ in uranyl minerals, in which the structural connectivity is an important factor, as is the charge of the structural unit and the charge and identity of any interstitial complex present in the structure (Burns et al., 2004; Burns and Klingensmith, 2006; Klingensmith and Burns, 2007).

5.2.1. Carbonate minerals

Consistent with previous reports, we found that Np(V) is readily incorporated into calcite grown in aqueous solution under ambient conditions. The sharp reduction of the concentration of neptunium in the aqueous barrier solution subsequent to crystal nucleation, as shown by ICP-MS analyses, and the presence of substantial neptunium in the crystals, as shown by LA-ICP-MS analyses, demonstrate incorporation of Np(V) in calcite (Figure 3, Table 1). Np(V) as the $(Np_2O)^+$ neptunyl ion may substitute for Ca^{2+} in calcite, as reported earlier (Heberling et al., 2008). We find that Np(V) neptunyl is incorporated into calcite at much higher levels than U(VI) uranyl, under otherwise identical synthetic conditions. This is despite the requirement of a charge-balancing mechanism in the case of Np(V) neptunyl substitution for calcium. This disparity may be due to the different sizes and charges of $(UO_2)^{2+}$ and $(NpO_2)^+$, or to different affinities of the uranyl and neptunyl ions with carbonate complexes, U(VI) being most likely present as $UO_2(CO_3)_3^{4-}$ and Np(V) as NpO_2^+ or $NpCO_3^-$ under the conditions of crystal growth.

By considering the differences in actinide uptake into calcite and aragonite, we have probed the impact of structural differences on incorporation of U(VI) uranyl or Np(V) neptunyl. Previous studies of U(VI) uranyl incorporation in aragonite indicate a higher level of incorporation may occur than in calcite, possibly due to fewer coordination constraints in the case of aragonite (Kelly et al., 2006; Reeder et al., 2000). In particular, the aragonite structure is consistent with incorporation of the $UO_2(CO_3)_3^{4-}$ geometrical unit (Reeder et al., 2000), but calcite is not. The Ca^{2+} in calcite is octahedrally coordinated by six monodentate carbonate, whereas the less regular and larger Ca^{2+} environment in aragonite contains three bidentate carbonate units. Our study reveals a higher level of U(VI) incorporation in aragonite, as compared to calcite, with both crystallized from similar aqueous systems under ambient conditions. The luminescence spectrum of U(VI) uranyl in aragonite (Figure 7) is consistent with the presence of a uranyl-triscarbonato unit, as reported by Reeder et al. (2000, 2001). Our results also indicate that aragonite can incorporate as much as ~3000 ppm of Np(V) neptunyl (Table 1), a level that is similar to U(VI) uranyl incorporated in aragonite in our experiments.

Strontianite, cerussite, celestine, and anglesite are isostructural with aragonite, prompting us to select these minerals for study to examine the impact of the size of the divalent cation site, as well as the presence of either carbonate or sulfate oxyanions, on Np(V) neptunyl and U(VI) uranyl incorporation.

The experimental data for strontianite and cerussite confirm uptake of both U(VI) and Np(V) from solution, although to different extents. As much as 90-98% of the Np(V) and U(VI) in the barrier solution of the strontianite synthesis is removed by Day 3. For

cerussite, 20 - 40% of U(VI) or Np(V) are removed from solution by Day 3 in experiments at either low or high actinide concentrations (Figure 3, Figure SI 5). By day 7, 78-80 % of the total U(VI) or Np(V) has been removed from solution (Figure 3). The strontianite and cerussite powders were washed using ultrapure water, and analyses of this aqueous solution following contact with the product revealed that ~25-40% of the U(VI) and Np(V) associated with cerussite are released back into solution. This is not the case for strontianite, which indicates that U(VI) and Np(V) more strongly interact with the strontianite powders. Note that the lack of single crystals of strontianite and cerrusite prevents the application of LA-ICP-MS to definitively demonstrate incorporation of the actinyl ions.

Incorporation of U(VI) in strontianite or cerussite could occur in a coordination environment similar to that of aragonite. In this case, the luminescence spectra of U(VI) uranyl incorporated in these minerals would display similar spectral features, as luminescence emission spectra are sensitive to slight changes in coordination environments about U(VI). The luminescence spectrum of U(VI)-doped strontianite powder displays similar spectral features as the U(VI)-doped aragonite, although the peak positions are red shifted by 2-7 nm in the strontianite spectrum (Figure 7). The Sr-O bonds in strontianite are ~0.15 Å longer that the Ca-O bonds in aragonite, perhaps providing a more relaxed coordination environment about U(VI) in strontianite, consistent with the observed red shifts. Aside from the red shift, the luminescence spectrum indicates that U(VI) incorporated in strontianite has a similar coordination environment as in aragonite, presumably as a triscarbonato unit. On the other hand, the luminescence spectrum of U(VI)-doped cerussite differs significantly from U(VI)-bearing

aragonite and strontianite in that the peaks are sharper with peak maxima red-shifted by ~ 15 nm, and the spectral feature at ~570 nm is absent. The time resolved spectra are rather different from the long-lived species observed for either aragonite or strontianite, with the long-lived species for cerussite containing better resolved vibronic features (Figure 7). This indicates major structural differences in the U(VI) environment in cerussite, relative to the other aragonite-structure minerals under study. The luminescence spectra of U(VI) in cerussite display features that are inconsistent with incorporated uranyl-carbonato species, although they resemble spectral features of uranyl oxy-hydrate minerals. Reference luminescence spectra of uranyl carbonate and hydroxide minerals collected under the same experimental conditions are reported in the Supplementary Information for comparison (Figure SI 9).

U(VI)-doped and Np(V)-doped cerussite samples were imaged and analyzed using scanning transmission electron microscopy (TEM), high resolution TEM, and energy dispersive X-ray spectroscopy (EDS). Both uranium and neptunium were found on the surface of cerussite grains using TEM with EDS. The high-resolution TEM images of the U(VI) material gave a *d*-spacing of 2.82 - 2.88 Å, which does not correspond to any major *d*-spacing of cerussite. This indicates the presence of a secondary crystalline phase on the surface of the cerussite grains, although definitive identification of the phase is not possible. Schoepite $[(UO_2)_8O_2(OH)_{12}](H_2O)_{12}$, rutherfordine ($UO_2CO_3$), or a Pb-uranyl oxyhdrate are possible crystalline phases that may have precipitated in the cerussite synthesis system considering the uranyl concentration, pH (Tokunaga et al., 2012) and composition of the solution. The *d*-spacing of 2.82 -2.88 Å is consistent with dehydrated-schoepite ($UO_3.H_2O$, PDF # 00-010-0322) or curite

($Pb_3(UO_2)_8O_8(OH)_6.3(H_2O)$, PDF # 00-051-1531), and the dehydration of schoepite is expected in the vacuum of the TEM.

A Np-bearing phase was also imaged on the surface of cerussite, although no lattice fringes were resolved. The Np(V) concentration in the barrier solution is below the Np_2O_5 solubility limit, but the chemical gradient dictated by the synthesis apparatus could provide local environments favoring precipitation, such as in the vicinity of the ammonium carbonate-bearing 2.5mL-vial. EDS spectra together with high-resolution TEM images, are in the Supporting Information (Figure SI 11, Figure SI 12).

Data collected for strontianite and cerrusite by ICP-MS, cryogenic luminescence spectroscopy, and TEM taken together indicate that whereas the strontium site in strontianite may be a good host for structural incorporation of Np(V) and U(VI), the Pb site of cerussite is not. The slower uptake of U(VI) and Np(V) by the cerussite product, together with TEM imaging evidence of Np or U bearing precipitates on the mineral grains, indicate that cerussite does not incorporate significant Np(V) or U(VI), under the experimental conditions. Rather, removal of U(VI) or Np(V) from synthetic solutions forming cerussite is likely the result of either surface adsorption or precipitation of a secondary phase (either secondary mineral or colloidal precipitates).

5.2.2. Sulfate minerals

The ICP-MS solution data gathered for samples of barrier solutions from the synthesis of celestine and anglesite indicate no significant decrease of Np or U in solution during crystal growth (Figure 4). LA-ICP-MS data confirm the low or non-existent level of incorporation of U(VI) and Np(V) in celestine (10 - 50ppm), with Np(V) present at

about double the concentration of uranium (Table 1). LA-ICP-MS data for anglesite indicate a low uptake of Np(V) (~ 10 ppm average) only in those crystals synthesized at high Np(V) concentrations (Table 1).

TRLFS data collected for U(VI)-doped celestine indicates a single U(VI) site (Figure 8), with peak maxima characteristic of uranyl coordinated by monodentate sulfate (Vercouter et al., 2008). Consistent with LA-ICP-MS data that showed a lack of interaction between U(VI) and anglesite, luminescence measurements of anglesite show no luminescence (Figure SI 8).

Data obtained for strontium and lead carbonate and sulfate minerals in this work indicate that whereas the Sr^{2+} site may be favorable for actinide substitution in the aragonite-type crystal lattice, the Pb^{2+} site is not a favorable environment. This may be attributed to the larger ionic radius of Pb or the typical stereoactive lone-electron pair behavior of Pb^{2+}.

The experimental data for gypsum do not rigorously demonstrate incorporation of either U(VI) or Np(V). Data gathered from LA-ICP-MS suggests that both Np(V) and U(VI) are present only at or near the surface (Figure SI 7). Cryogenic luminescence spectra indicate the presence of multiple U(VI) environments (Figure 8). The long-lived components display nicely resolved sharp peaks that are characteristics typically displayed by spectra of uranyl minerals, rather than incorporated species. The presence of multiple U(VI) environments may indicate that some of the U(VI) is sorbed on the gypsum surface, and that some may have nucleated as a secondary mineral, such as bequerelite.

5.3. Incorporation models

Hypothetical models based on the steric constraints of the crystal structures of the mineral phases considered in this work provide insight concerning the potential host sites for actinyl ions. In the structure of calcite, calcium is coordinated by six monodentate CO_3^{2-} units with Ca-O bond distances of ~2.35 Å. The neptunyl Np(V) ion could fit into the calcite structure via a direct substitution of NpO_2^+ for Ca^{2+}, as a Np(V) cation for Ca^{2+}, or a combination of both of these (Figure 10 a, b). In calcite, substitution of Ca^{2+} by divalent cations is common, but substitution by NpO_2^+ would require structure flexibility and a mechanism to achieve charge balance. The uranyl triscarbonato unit, $(UO_2(CO_3)_3)^{4-}$, is the most favored U(VI) carbonate complex in solution (Clark et al., 1995; Silva and Nitsche, 1995) and the solid state (Burns, 2005). In uranyl carbonate minerals, U(VI) is usually present in a hexagonal bipyramid coordination environment in which three bidentate carbonate units form three equatorial edges of the bipyramid (Burns, 2005). The steric constraints of the Ca^{2+} site in calcite prohibit the incorporation of the $(UO_2(CO_3)_3)^{4-}$ unit, but it is possible in aragonite.

Three approximately coplanar bidentate carbonate units and two monodentate carbonate units coordinate the calcium site in the aragonite structure (Figure 10 d), with average Ca-O bond distances of ~2.53 Å. As previously discussed by Reeder et al. (2000), the steric constraints of the coordinating ligands about the Ca^{2+} site in aragonite permit it to accommodate the $(UO_2(CO_3)_3)^{4-}$ unit (Figure 10 c). Our experimental results indicate that the aragonite structure can accommodate both U(VI) and Np(V). In the few Np(V) carbonate compounds with known structures, $(NpO_2)^+$ is present in hexagonal bipyramids with one bidentate carbonate unit (Volkov et al., 1979). These observations

indicate that $(NpO_2)^+$ may not favor a particular coordination involving specific arrangements of CO_3^{2-} units, allowing more flexibility for incorporation. In the structure of aragonite, $(NpO_2)^+$ could be incorporated as $NpO_2(CO_3)_3^{5-}$ with three bidentate carbonate units in the equatorial plane, or coordinated by five monodentate carbonate units (Figure 10 c, d). The structure of strontianite may accommodate Np(V) and U(VI) in a similar coordination environment as aragonite (Figure 10 c, d). The Sr-O bond distances are ~0.1Å longer than the Ca-O distances in aragonite, allowing some structural relaxation.

Experimental data do not support incorporation of either U(VI) uranyl or Np(V) neptunyl in the structure of cerussite. The Pb-O bond distances in cerussite are 0.16 Å longer than Ca-O and 0.06 Å longer than Sr-O in strontianite.

Aragonite-structured celestine and anglesite have larger unit cell parameters, metal-to-oxygen distances, and unit cell volumes than their carbonate counterparts due to the presence of $(SO_4)^{2-}$ rather than $(CO_3)^{2-}$. In celestine and anglesite, Sr^{2+} and Pb^{2+} are coordinated by three bidentate sulfate groups and two oxygen atoms from monodentate sulfate groups (Figure 11a). Sr-O bond lengths range between 2.523(2) and 3.260(1) Å, with an average bond length of 2.82 Å. Pb-O bond lengths range between 2.609(7) and 3.271(4) Å, with an average bond length of ~2.86 Å. Considering bond length and geometry constraints, the most favorable U(VI) and Np(V) coordination in these structures would be as an actinyl unit in a pentagonal bipyramid involving five monodentate oxygen atoms from sulfate units, as shown in Figure 11b. In U(VI) and Np(V) sulfates, the actinyl unit is usually present in a pentagonal bipyramidal coordination environment that includes oxygen atoms from monodentate or bidentate

sulfate tetrahedra (Burns, 2005; Forbes et al., 2008; Neuefeind et al., 2004), consistent with the coordination of the actinyl unit proposed in Figure 11b. Experimental data gathered for celestine and anglesite here indicate that the incorporation of neptunium, although low, is favored over uranium. Slightly longer neptunyl bipyramid equatorial bond lengths, as compared to uranyl, may explain this preferential uptake. The presence of three bidentate sulfate groups in the Ca^{2+} coordination environment may be important during actinyl incorporation at this site owing to cation-cation repulsion. The S(VI)-U(VI)/Np(V) repulsion would be more important than the C(IV)-U(VI)/Np(V) repsulsion in the case of aragonite, and would be most severe for U(VI). Although uranyl ions coordinated by a single bidentate sulfate are known in the solid state, none are known in which there are two or more bidentate sulfate groups coordinating uranyl (Burns, 2005).

In the monoclinic structure of gypsum, each calcium site is coordinated by two oxygen atoms from monodentate sulfate groups, two oxygen atoms of each of two bidentate sulfate groups, and two water molecules (Figure 11c). Although isomorphous substitution for Ca^{2+} does occur (Shen et al., 2001), the most common variation in gypsum chemistry is dehydration to anhydrite, $CaSO_4$. In gypsum, due to geometrical constraints, the substitution of uranyl or neptunyl for calcium would require the $(SO_4)^{2-}$ groups to move in a way that would destroy the integrity of the structure. Specifically, to maintain the coordination of the coplanar oxygen atoms in the equatorial plane of the actinyl unit coordination polyhedron, an oxygen atom from a bidentate sulfate group would be lost.

6. Conclusions

Co-precipitation of Np(V) or U(VI) actinyl ions into low-temperature mineral structures in the subsurface is one mechanism that may limit their mobility, or that could be encouraged in a groundwater remediation strategy. Our hypothesis that the behaviors of Np(V) neptunyl and U(VI) uranyl towards incorporation in a variety of mineral structures would show disparity despite the similar geometries of these units is supported by the findings herein. Specifically, dramatically different incorporation levels are found for U(VI) and Np(V) in carbonate minerals grown from very similar aqueous solutions under ambient conditions. These results clearly demonstrate, as others have in the past, that the crystal-chemical behaviors of Np(V) and U(VI) actinyl ions are sufficiently different that predictions concerning the fate of Np(V) based on experience with U(VI) are likely to be erroneous. These results also indicate that the coprecipitation of Np(V) into mineral structures could reduce its mobility in the subsurface.

Acknowledgements

This research was funded by the United States Department of Energy, Office of Biological & Environmental Research, Subsurface Geochemical Research Program, grant DOE-DE-SC0004245. This work was performed in part at the William R. Wiley Environmental Science Laboratory (EMSL), a national scientific user facility sponsored by the U.S. Department of Energy's Office of Biological and Environmental Research and located at the Pacific Northwest National Laboratory, operated for the Department of Energy by Battelle.

References

1. Bruno, J.; Ewing, R. C. Spent nuclear fuel. *Elements* **2006**, *2*, 343-349.

2. Burns, P. C.; Klingensmith, A. L. Uranium mineralogy and neptunium mobility. *Elements* **2006**, *2*, 351-356.

3. Finch, R.; Buck, E.; Finn, P.; Bates, J. Oxidative corrosion of spent UO2 fuel in vapor and dripping groundwater at 90 degrees C. **1999**, *556*, 431-438.

4. Forbes, T.; Wallace, C.; Burns, P. Neptunyl Compounds: Polyhedron Geometries, Bond-Valence Parameters, and Structural Hierarchy. *Can. Mineral.* **2008**, *46*, 1623-1645.

5. Antonio, M.; Soderholm, L.; Williams, C.; Blaudeau, J.; Bursten, B. Neptunium redox speciation. *Radiochim Acta* **2001**, *89*, 17-25.

6. Efurd, D. W.; Runde, W.; Banar, J.; Janecky, D.; Kaszuba, J.; Palmer, P.; Roensch, F.; Tait, C. D. Neptunium and Plutonium Solubilities in a Yucca Mountain Groundwater. *Environmental science technology* **1998**, *32*, 3893-3900.

7. Burns, P. C.; Ewing, R. C.; Navrotsky, A. Nuclear Fuel in a Reactor Accident. *Science* **2012**, *335*, 1184-1188.

8. Burns, P. C. U6+ minerals and inorganic compounds: Insights into an expanded structural hierarchy of crystal structures. *Canadian Mineralogist* **2005**, *43*, 1839-1894.

9. Clark, D.; Hobart, D.; Neu, M. Actinide Carbonate Complexes and their Importance in Actinide Environmental Chemistry. *Chem. Rev.* **1995**, *95*, 25-48.

10. Altmaier, M.; Gaona, X.; Fanghaenel, T. Recent Advances in Aqueous Actinide Chemistry and Thermodynamics. *Chem. Rev.* **2013**, *113*, 901-943.

11. Maher, K.; Bargar, J. R.; Brown, G. E., Jr. Environmental Speciation of Actinides. *Inorg. Chem.* **2013**, *52*, 3510-3532.

12. Katz, J. J.; Morss, L. R.; Edelstein, N. M.; Fuger, J. Introduction. **2006**, 1-17.

13. Serezhkin, V. N.; Sidorenko, G. V.; Pushkin, D. V.; Serezhkina, L. B. Cation-cation interactions between uranyl(VI) ions. *Radiochemistry* **2014**, *56*, 115-133.

14. Sullivan, J.; Zielen, A.; HIindman, J. SPECIFIC INTERACTION BETWEEN NP(V) AND U(VI) IN AQUEOUS PERCHLORIC ACID MEDIA. *J. Am. Chem. Soc.* **1961**, *83*, 3373.

15. Curti, E. Coprecipitation of radionuclides with calcite: estimation of partition coefficients based on a review of laboratory investigations and geochemical data. *Appl. Geochem.* **1999**, *14*, 433-445.

16. Kaszuba, J.; Runde, W. The aqueous geochemistry of neptunium: Dynamic control of soluble concentrations with applications to nuclear waste disposal. *Environmental science {\&} technology* **1999**, *33*, 4427-4433.

17. Burns, P.; Deely, K.; Skanthakumar, S. Neptunium incorporation into uranyl compounds that form as alteration products of spent nuclear fuel: Implications for geologic repository performance. *Radiochimica Acta* **2004**, *92*, 151-159.

18. Alessi, D. S.; Szymanowski, J. E. S.; Forbes, T. Z.; Quicksall, A. N.; Sigmon, G. E.; Burns, P. C.; Fein, J. B. Mineralogic controls on aqueous neptunium(V) concentrations in silicate systems. *J. Nucl. Mater.* **2013**, *433*, 233-239.

19. Forbes, T. Z.; Burns, P. C. Ba(NpO2)(PO4)(H2O), its relationship to the uranophane group, and implications for Np incorporation in uranyl minerals. *Am. Mineral.* **2006**, *91*, 1089-1093.

20. Kelly, S.; Rasbury, E.; Chattopadhyay, S.; Kropf, A.; Kemner, K. Evidence of a stable uranyl site in ancient organic-rich calcite. *Environ. Sci. Technol.* **2006**, *40*, 2262-2268.

21. Reeder, R.; Nugent, M.; Tait, C.; Morris, D.; Heald, S.; Beck, K.; Hess, W.; Lanzirotti, A. Coprecipitation of uranium(VI) with calcite: XAFS, micro-XAS, and luminescence characterization. *Geochim. Cosmochim. Acta* **2001**, *65*, 3491-3503.

22. Reeder, R.; Nugent, M.; Lamble, G.; Tait, C.; Morris, D. Uranyl incorporation into calcite and aragonite: XAFS and luminescence studies. *Environmental science {\&} technology* **2000**, *34*, 638-644.

23. Reeder, R.; Elzinga, E.; Tait, C.; Rector, K.; Donohoe, R.; Morris, D. Site-specific incorporation of uranyl carbonate species at the calcite surface. *Geochim. Cosmochim. Acta* **2004**, *68*, 4799-4808.

24. Heberling, F.; Denecke, M. A.; Bosbach, D. Neptunium(V) coprecipitation with calcite. *Environ. Sci. Technol.* **2008**, *42*, 471-476.

25. Heberling, F.; Brendebach, B.; Bosbach, D. Neptunium(V) adsorption to calcite. *J. Contam. Hydrol.* **2008**, *102*, 246-252.

26. Heberling, F.; Scheinost, A. C.; Bosbach, D. Formation of a ternary neptunyl(V) biscarbonato inner-sphere sorption complex inhibits calcite growth rate. *J. Contam. Hydrol.* **2011**, *124*, 50-56.

27. Zavarin, M.; Roberts, S.; Hakem, N.; Sawvel, A.; Kersting, A. Eu(III), Sm(III), Np(V), Pu(V), and Pu(IV) sokption to calcite. *Radiochimica Acta* **2005**, *93*, 93-102.

28. Fernandes, M. M.; Schmidt, M.; Stumpf, T.; Walther, C.; Bosbach, D. Site-selective time-resolved laser luminescence spectroscopy of Eu3 in calcite. *J. Colloid Interface Sci.* **2008**, *321*, 323-331.

29. Schmidt, M.; Stumpf, T.; Walther, C.; Geckeis, H.; Fanghaenel, T. Incorporation versus adsorption: substitution of Ca(2) by Eu(3) and Cm(3) in aragonite and gypsum. *Dalton transactions* **2009**, 6645-6650.

30. Holliday, K.; Chagneau, A.; Schmidt, M.; Claret, F.; Schaefer, T. Discriminating factors affecting incorporation: comparison of the fate of Eu3 -Cm3 in the Sr carbonate-sulfate system. *Dalton transactions* **2012**, *41*, 3642-3647.

31. Franke, W.; Lenk, K.; Ittyachen, M.; Pillai, K. The Morphology of Cerussite Pbco3 Grown in Silica-Gel and on Hydrothermal Conditions. *J. Cryst. Growth* **1981**, *51*, 309-313.

32. McCauley, J.; Roy, R. Controlled Nucleation and Crystal-Growth of various Caco3 Phases by Silica-Gel Technique. *Am. Mineral.* **1974**, *59*, 947-963.

33. Fernandez-Diaz, L.; Astilleros, J.; Pina, C. The morphology of calcite crystals grown in a porous medium doped with divalent cations. *Chem. Geol.* **2006**, *225*, 314-321.

34. Locock, A.; Burns, P. Crystal structures and synthesis of the copper-dominant members of the autunite and meta-autunite groups: Torbernite, zeunerite, metatorbernite and metazeunerite. *Canadian Mineralogist* **2003**, *41*, 489-502.

35. Locock, A.; Kinman, W.; Burns, P. The structure and composition of uranospathite A11-x square(x)[(UO2)(PO4)](2)(H2O)(20+3x)F1-3x, 0 < x < 0.33, a non-centrosymmetric flourine-bearing mineral of the autunite group, and of a related synthetic lower hydrate, Al-0.67 square(0.33)[(UO2)(PO4)](2)(H2O)(15.5). *Canadian Mineralogist* **2005**, *43*, 989-1003.

36. Fernelius, W. C.; Detling, K. D. Preparation of crystals of sparingly soluble salts. *J. Chem. Educ.* **1934**, *11*, 176.

37. Engelhard, M.; Baer, D. Vacuum Cleaved Calcium Carbonate by XPS. *Surface Science Spectra* **1999**, *6*, 153-159.

38. Vercouter, T.; Vitorge, P.; Amekraz, B.; Moulin, C. Stoichiometries and thermodynamic stabilities for aqueous sulfate complexes of U(VI). *Inorg. Chem.* **2008**, *47*, 2180-2189.

39. Teterin, A. Y.; Mikhailina, A. V.; Maslakov, K. I.; Zaharova, E. V.; Teterin, Y. A. The Xps Study of Physical and Chemical Forms of Neptunium Group on the Surface of Minerals. *Nuclear Technology & Radiation Protection* **2010**, *25*, 1-7.

40. Hennig, C.; Ikeda Ohno, A.; Tsushima, S.; Scheinost, A. The sulfate coordination of Np(IV), Np(V), and Np(VI) in aqueous solution. *Inorg. Chem.* **2009**, *48*, 5350-60.

41. Neuefeind, J.; Skanthakumar, S.; Soderholm, L. Structure of the UO2 2 -SO 4 2- ion pair in aqueous solution. *Inorg. Chem.* **2004**, *43*, 2422-6.

42. Silva, R.; Nitsche, H. Actinide environmental chemistry. *Radiochim. Acta* **1995**, *70-1*, 377-396.

43. Runde W. Spectroscopies for environmental studies of actinide species. *Chemical Interactions of Actide in the environment, Los Alamos Science* **2000**, *26*.

44. Vallet, V.; Wahlgren, U.; Grenthe, I. Probing the Nature of Chemical Bonding in Uranyl(VI) Complexes with Quantum Chemical Methods. *Journal of Physical Chemistry a* **2012**, *116*, 12373-12380.

45. Klingensmith, A. L.; Burns, P. C. Neptunium substitution in synthetic uranophane and soddyite. *Am. Mineral.* **2007**, *92*, 1946-1951.

46. Tokunaga, T.; Kim, Y.; Wan, J.; Yang, L. Aqueous uranium(VI) concentrations controlled by calcium uranyl vanadate precipitates. *Environmental science technology* **2012**, *46*, 7471-7.

47. Volkov, Y.; Tomilin, S.; Visyaschcheva, G.; Kapshukov, I. Study of carbonate compounds of pentavalenta actinides with alkali metal cations. VI. X-ray diffraction study of lithium

monocarbonatoneptunate ($LiNpO_2CO_3$) and sodium monocarbonatoneptunate ($NaNpO_2CO_3$). *Radiochim. Acta* **1979**, *26*, 668–672.

18. Shen, Y.; Buick, R.; Canfield, D. E. Isotopic evidence for microbial sulphate reduction in the early Archaean era. *Nature* **2001**, *410*, 77–81.

Figure 1. Photograph (left) and schematic (right) of the apparatus used to synthesize actinyl carbonate crystals from aqueous solution. This apparatus was employed for the synthesis of all materials in this work.

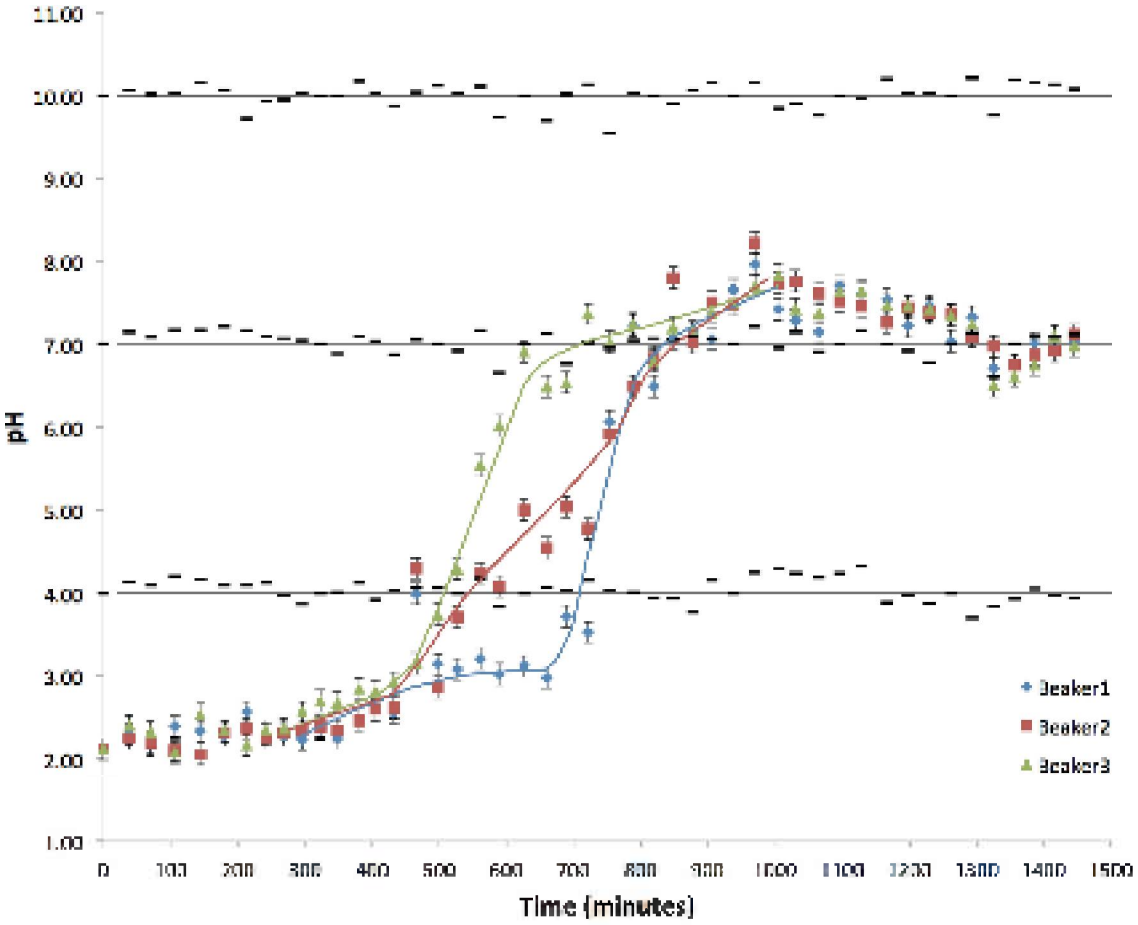

Figure 2 Measured pH of the aqueous barrier solution for the synthesis of calcite in three different beakers as a function of time. The synthesis experiments began using the apparatus shown in Figure 1, with a barrier solution pH = 2.2. The measured pH values of standard solutions are shown by black dashes. The three colored lines represent the approximate pH of the solutions through the region of rapidly changing pH.

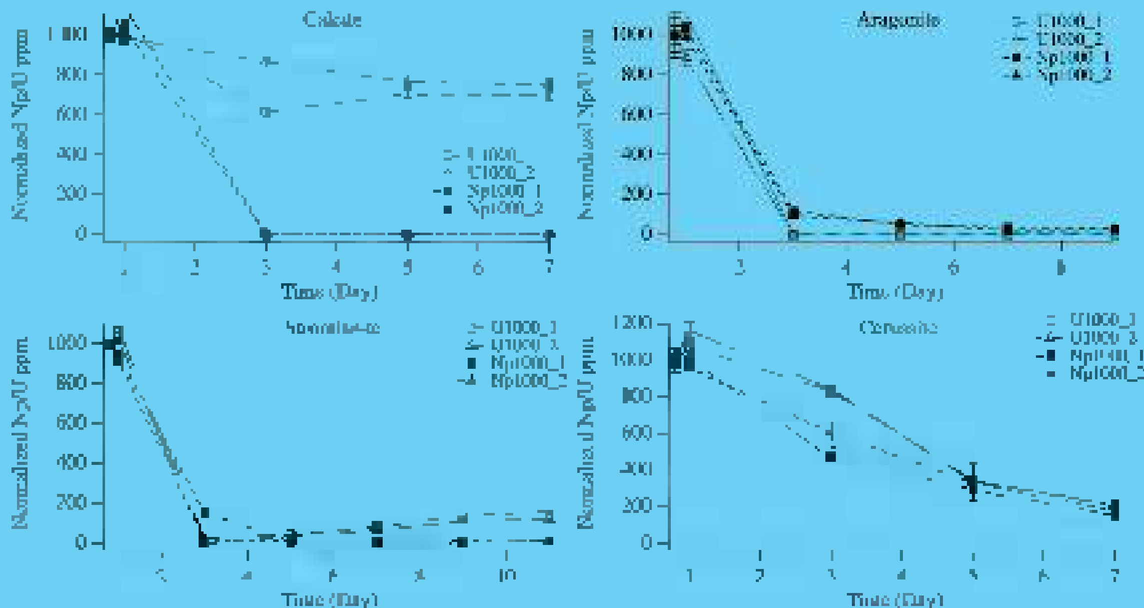

Figure 3 ICP-MS results for barrier solutions from which carbonate minerals were utilized. Data displayed for high concentration experiments (1000 ppm)

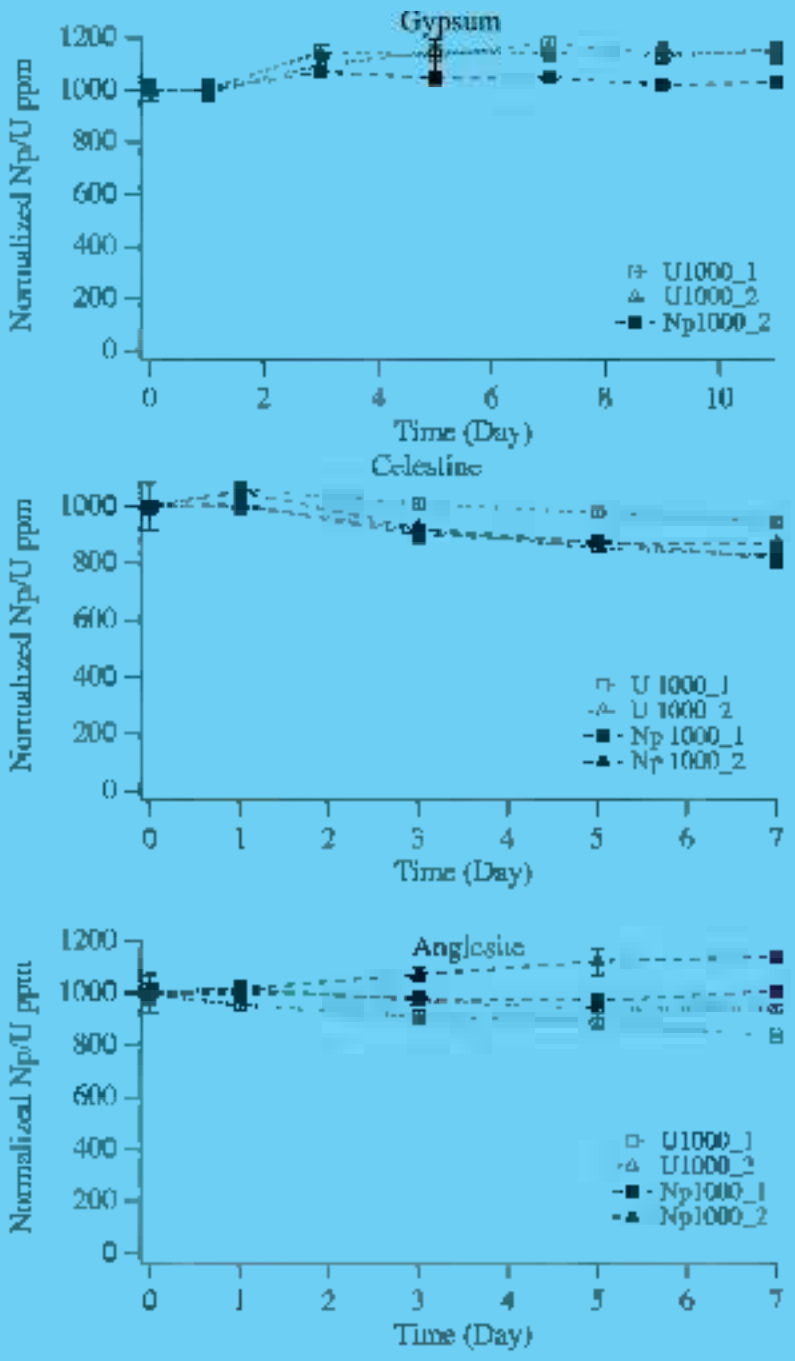

Figure 4 ICP-MS results for barium solutions from which sulfate minerals formed. Data displayed for high [U] and high [Np] experiments (1000 ppm).

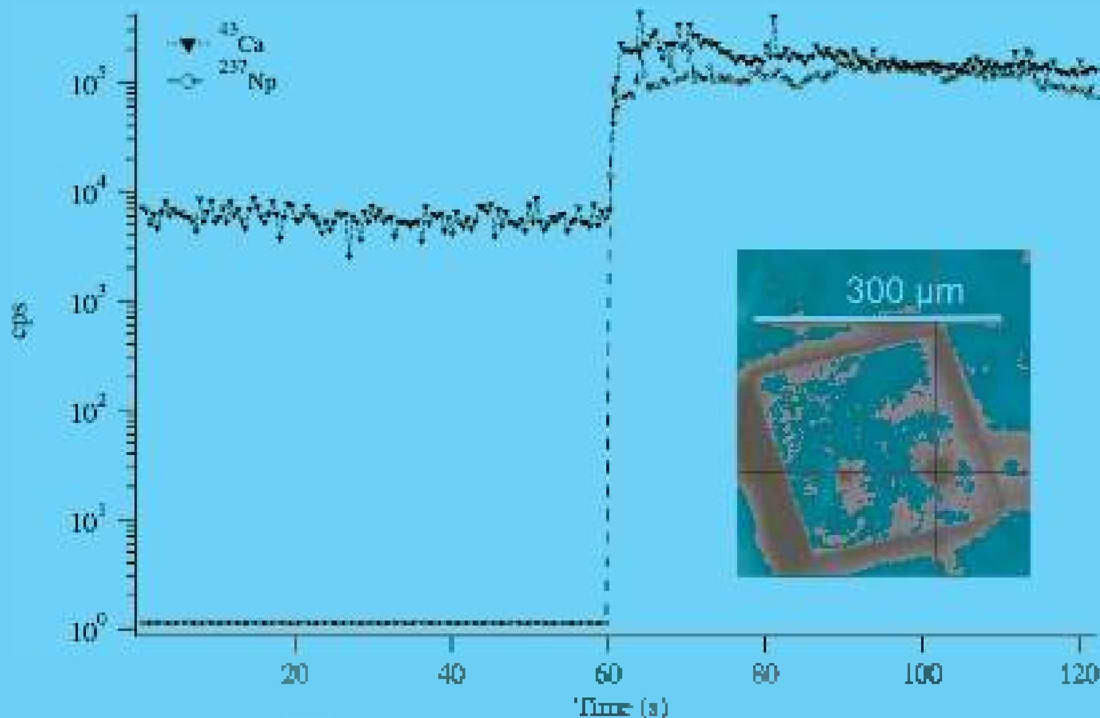

Figure [illegible]. LA-ICP-MS data for ^{43}Ca and ^{237}Np prior to laser ablation (left) and during laser ablation (right) of a calcite crystal (inset). Data were collected from material ablated from the crater that is visible on the lower-left side of the crystal.

Table 1 Concentration (ppm) of Np and U in different minerals calculated from LA-ICP-MS data. The average was calculated from data collected from ~15 crystals. The min and max value represent the lowest (*min*) and highest (*max*) concentration of each actinide for each set of crystals collected (nd= not detected; experiments with a Np doping of 8000 ppm were performed only for calcite).

	Np 400	**Np 1000**	**Np 8000**	**U 400**	**U 1000**
Calcite					
Average (ppm)	561	1101	3148	13	148
min (ppm)	*160*	*345*	*709*	*2*	*37*
max (ppm)	*1383*	*2252*	*5413*	*46*	*302*
Aragonite					
Average (ppm)	813	1628	-	794	1437
min (ppm)	*621*	*123*	-	*406*	*774*
max (ppm)	*2066*	*3335*	-	*1812*	*2063*
Celestine					
Average (ppm)	23	53	-	10	13
min (ppm)	*13*	*25*	-	*4*	*7*
max (ppm)	*38*	*90*	-	*21*	*30*
Anglesite					
Average (ppm)	*nd*	8	-	*nd*	*nd*
min (ppm)	*nd*	*3*	-	*nd*	*nd*
max (ppm)	*nd*	*25*	-	*nd*	*nd*

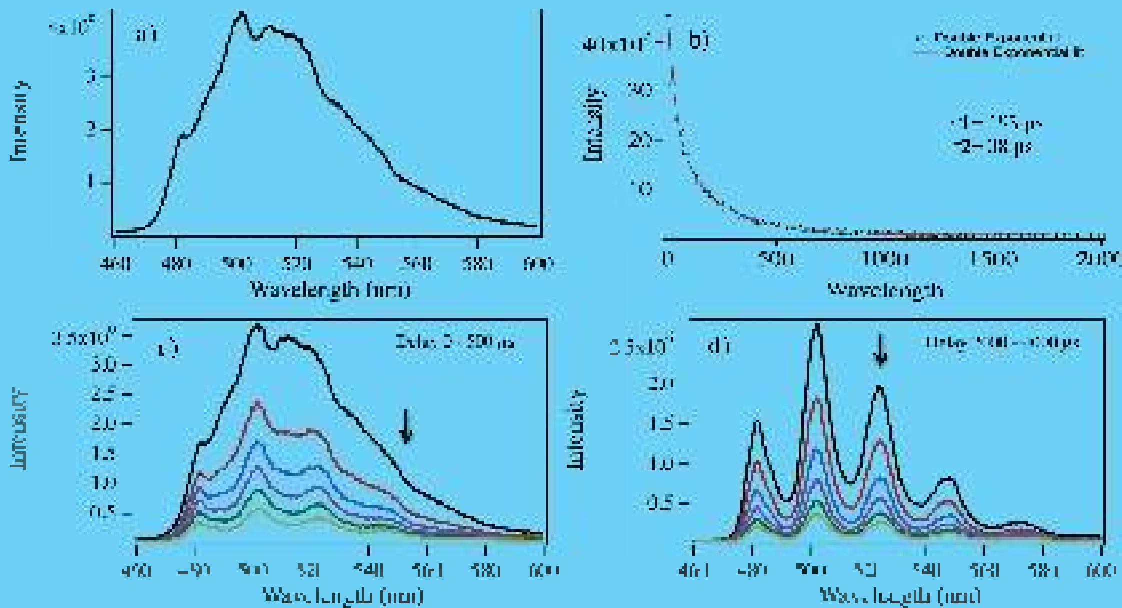

Figure 6 Luminescence spectra of uranyl-bearing calcite at 10K. λex = 415 nm. a) Luminescence spectra, b) decay kinetics, c) Time resolved luminescence emission spectra of short-lived components measured from [illegible] ps to [illegible] ps with a 100 ps interval, d) Time resolved luminescence emission spectra of long-lived components measured from 2000 ps to 4000 ps with a 400 ps interval. The arrows in c) and d) indicate the direction of delay time among the selected spectra.

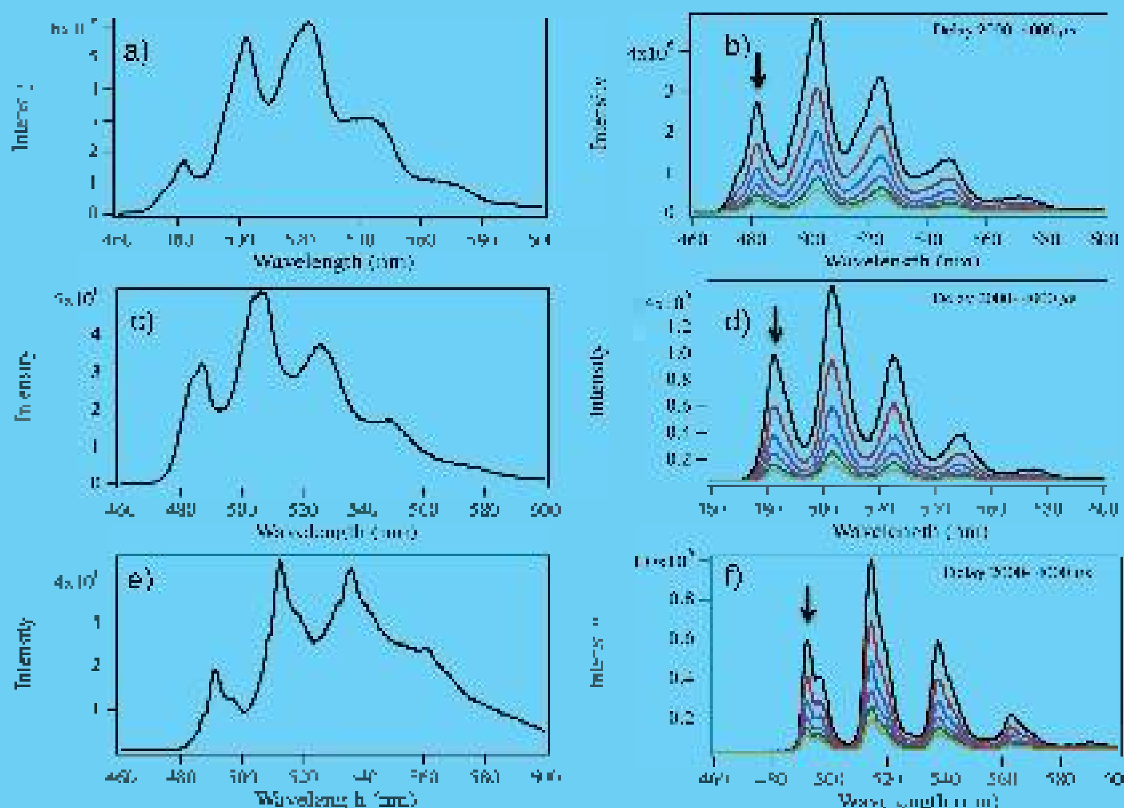

Figure 7. Luminescence spectra of uranyl-bearing aragonite (a, b), strontianite (c, d) and cerussite (e, f) at [illegible], λex = [illegible] nm. a), c), e) [illegible] luminescence spectra; b), d), f) time-resolved luminescence emission spectra of long lived components measured from 2000 ns to 1000 μs with a [illegible] μs interval. The arrows in b), d) and f) indicate the direction of delay time [illegible] the [illegible] spectra.

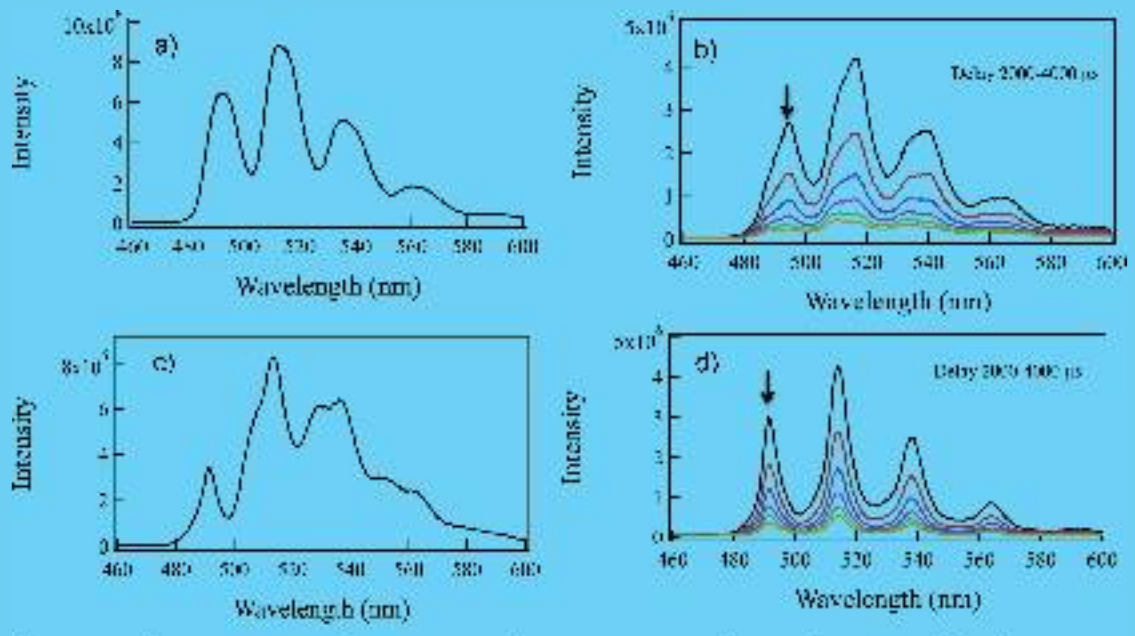

Figure 8. Luminescence spectra for cesium (a, b) and potassium (c, d) grown from nitrate bearing aqueous solution, with conditions at 10K (λ_{ex} = 355 nm). (a), (c) Platinum luminescence spectra. (b), (d) Time resolved luminescence emission spectra at long-lived components measured from 2000 µs to ~4000 µs with a 400 µs interval. The arrows in (b) and (d) indicate the direction of delay time during the shown spectra.

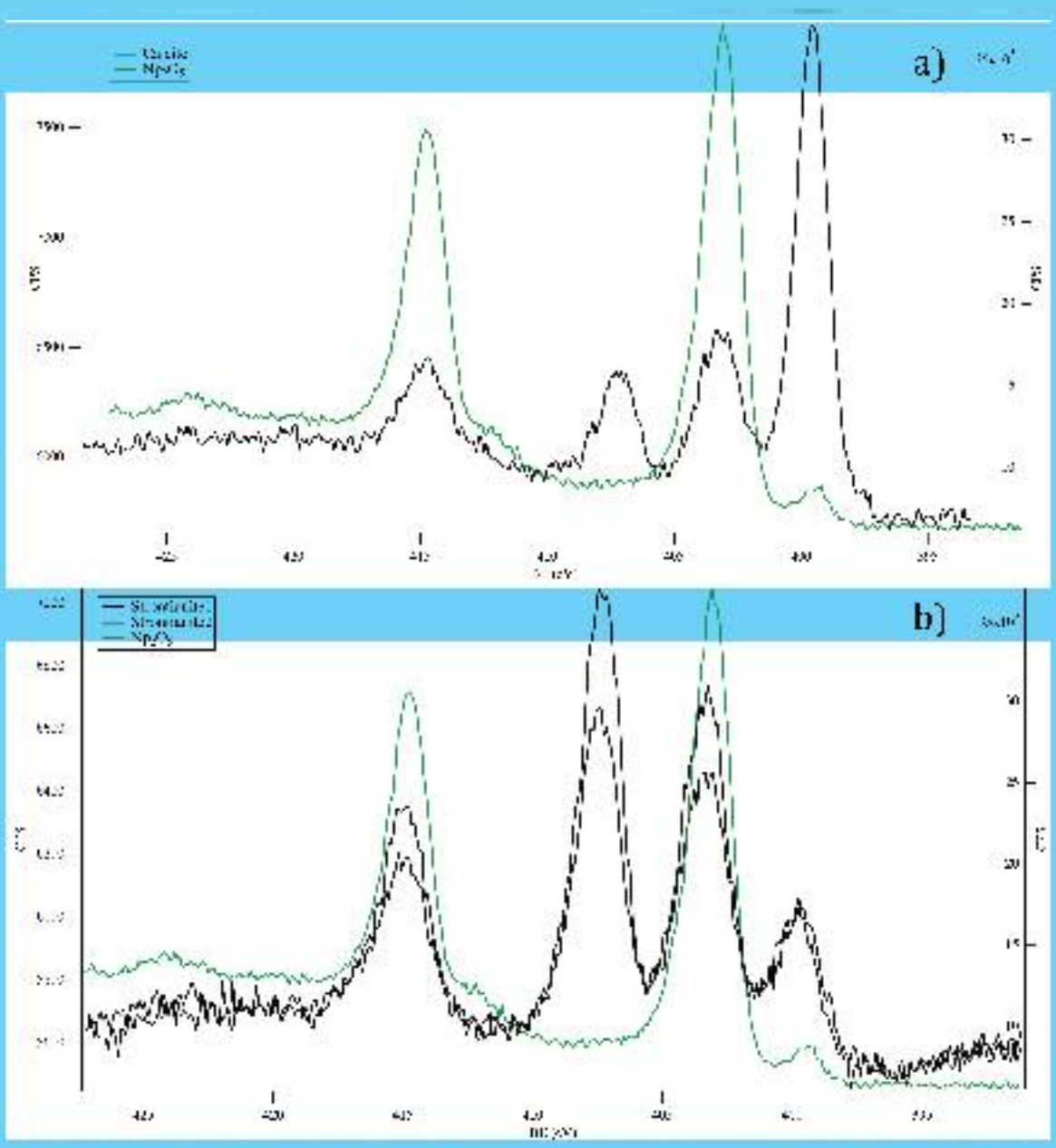

Figure 9: X-ray photoelectron spectra of Nb bearing calcite (a) and strontianite (b) compared to the Np_2O_5 standard. The two peaks at ~399 and ~404 eV in the calcite and strontianite spectra are attributed to the sorbed nitrogen species (N1s peak). The two peaks at ~414.7 and 403.5 eV correspond to the binding energy characteristic of Np_2O_5.

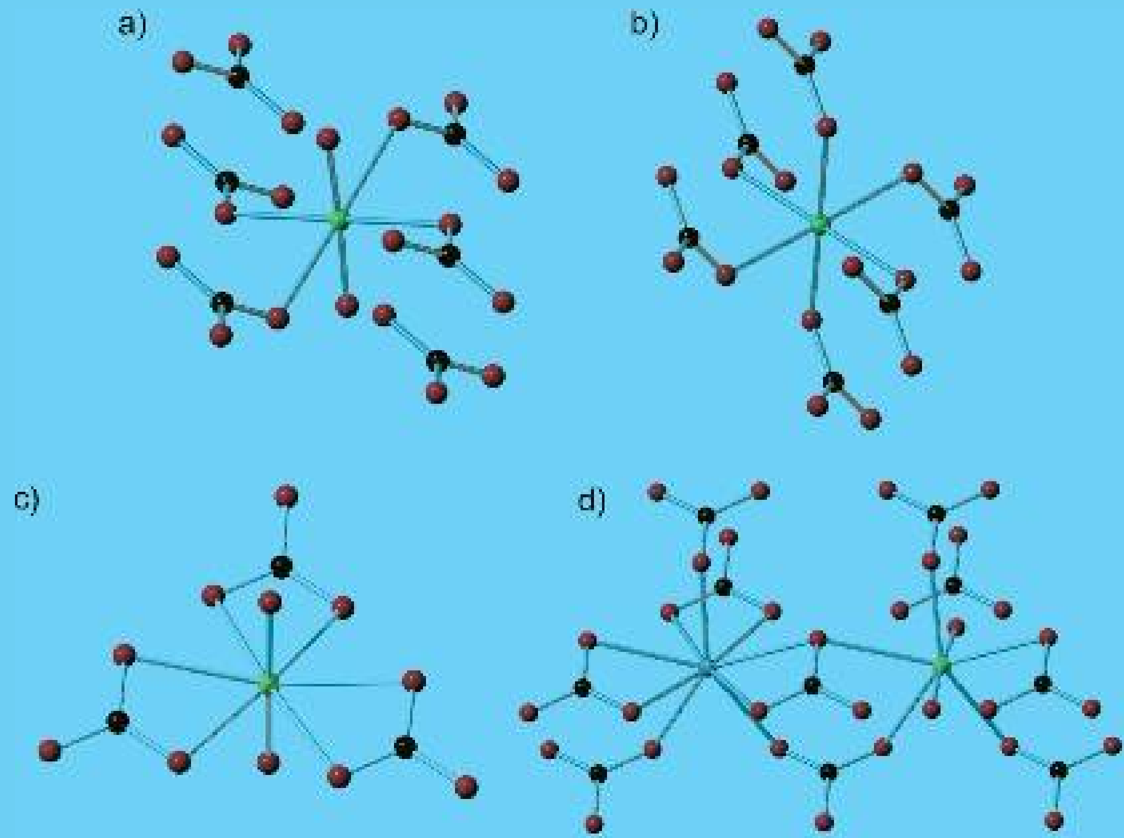

Figure 16 Structural models for incorporation of Np(V) into calcite (a and b) and U(VI) and Np(V) into aragonite (c and d). Calcite an NpO_2^+ is coordinated by four CO_3^{2-} units; but in neptunyl aragonite, Np^{5+} is coordinated by six CO_3^{2-} triangles with two extended bonds and four shorter bonds. (c) Aragonite [illegible] the $(UO_2(CO_3)_3)^{4-}$ unit can directly substitute for Ca in the structure of aragonite. (d) the calcium in the structure of aragonite is displayed in blue. The green is neptunium atom coordinated by two axial oxygen atoms and five monodentate carbonate units in the equatorial plane of a pentagonal bipyramid. Np(V) [illegible] particular coordination with CO_3^{2-} units, and configurations [illegible] could allow for incorporation of Np(V) into the aragonite structure. These configurations are also compatible with substitution of Np(V) or U(VI) for strontium in the structure of strontianite ($SrCO_3$).

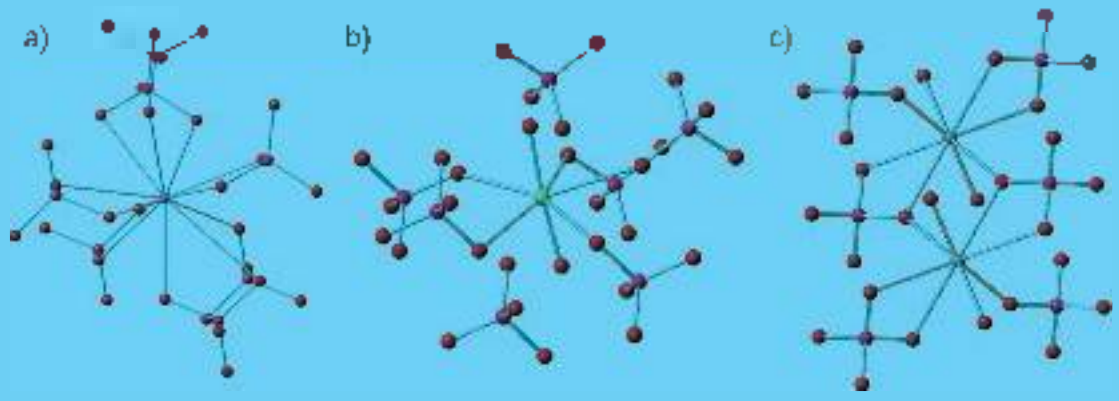

Figure 11 a) Cation coordination of Sr^{2+} and Pb^{2+} in the structures of celestine ($SrSO_4$) and anglesite ($PbSO_4$), b) Np(V) neptunate or U(VI) uranyl could replace Sr^{2+} by coordinating with five monodentate sulfate ions to form a pentagonal bipyramidal Ca^{2+} coordination of gypsum ($CaSO_4 \cdot 2H_2O$) and form a direct substitution due to geometrical constraints.

Table SI 1 Synthesis parameters for U and Np doped carbonate and sulfate minerals.

CALCITE	$CaCl_2$	$(NH_4)_2CO_3$	Barrier solution	U solution	Np solution
U- (400ppm)	1.5mL 1.7M	1.5mL 2.5M	I pH ~2.0 1M HCl	17µL 0.01M	
U- (1000 ppm)	1.5mL 1.7M	1.5mL 2.5M	I pH ~2.0 1M HCl	42 µL 0.01M	
Np- (400pppm)	1.5mL 1.7M	1.5mL 2.5M	I pH ~2.0 1M HCl		17µL 0.01M
Np- (1000 ppm)	1.5mL 1.7M	1.5mL 2.5M	I pH ~2.0 1M HCl		42 µL 0.01M
Np- (7500 ppm)	1.5mL 1.7M	1.5mL 2.5M	I pH ~2.0 1M HCl		315 µL 0.01M
ARAGONITE	$CaCl_2$	$(NH_4)_2CO_3$		U solution	Np solution
U- (400ppm)	1.5mL 1.7M	1.5mL 2.5M	I pH ~2.0 1M HCl in 0.125M $MgCl_2$	17µL 0.01M	
U- (1000 ppm)	1.5mL 1.7M	1.5mL 2.5M	I pH ~2.0 1M HCl in 0.125M $MgCl_2$	42 µL 0.01M	
Np- (400pppm)	1.5mL 1.7M	1.5mL 2.5M	I pH ~2.0 1M HCl in 0.125M $MgCl_2$		17µL 0.01M
Np- (1000 ppm)	1.5mL 1.7M	1.5mL 2.5M	I pH ~2.0 1M HCl in 0.125M $MgCl_2$		42 µL 0.01M
STRONTIANITE	$SrCl_2$	$(NH_4)_2CO_3$		U solution	Np solution
U- (400ppm)	1.5mL 2.4M	1.5mL 2.8M	I pH ~2.0 1M HCl	70 µL 0.03M	
U- (1000 ppm)	1.5mL 2.4M	1.5mL 2.8M	I pH ~2.0 1M HCl	150 µL 0.03M	
Np- (400pppm)	1.5mL 2.8M	1.5mL 2.8M	I pH ~2.0 1M HCl		70 µL 0.03M
Np- (1000 ppm)	1.5mL 2.8M	1.5mL 2.8M	I pH ~2.0 1M HCl		150 µL 0.03M
CERUSSITE	$PbNO_3$	$(NH_4)_2CO_3$		U solution	Np solution
U- (400ppm)	0.750mL 1.7M	0.750mL 2.5M	I pH ~2.0 1M HCl	17 µL 0.03M	
U- (1000 ppm)	0.750mL 1.7M	0.750mL 2.5M	I pH ~2.0 1M HCl	42 µL 0.03M	
Np- (400pppm)	0.750mL 1.7M	0.750mL 2.5M	I pH ~2.0 1M HCl		17µL 0.03M
Np- (1000 ppm)	0.750mL 1.7M	0.750mL 2.5M	I pH ~2.0 1M HCl		42 µL 0.03M
GYPSUM	$CaCl_2$	Na_2SO_4		U solution	Np solution
U- (400ppm)	1.5mL 1.7M	1.5mL 2.5M	I pH ~5.0 1M HCl	6 µL 0.1M	
U- (1000 ppm)	1.5mL 1.7M	1.5mL 2.5M	I pH ~5.0 1M HCl	16 µL 0.1M	
Np- (400pppm)	1.5mL 1.7M	1.5mL 2.5M	I pH ~5.0 1M HCl		59 µL 0.01M
Np- (1000 ppm)	1.5mL 1.7M	1.5mL 2.5M	I pH ~5.0 1M HCl		152 µL 0.01M
CELESTINE	$SrNO_3$	Na2SO4		U solution	Np solution
U- (400ppm)	1.6mL 1.7M	1.5mL 1.5M	I pH ~2.0 1M HCl	70 µL 0.03M	
U- (1000 ppm)	1.6mL 1.7M	1.5mL 1.5M	I pH ~2.0 1M HCl	185 µL 0.03M	
Np- (400pppm)	1.6mL 1.7M	1.5mL 1.5M	I pH ~2.0 1M HCl		70 µL 0.03M
Np- (1000 ppm)	1.6mL 1.7M	1.5mL 1.5M	I pH ~2.0 1M HCl		185 µL 0.03M
ANGLESITE	$PbNO_3$	$MgSO_4.(H_20)_7$		U solution	Np solution
U- (400ppm)	1.5mL 1.7M	1.5mL 2.4M	I pH ~2.0 1M HCl	70 µL 0.03M	
U- (1000 ppm)	1.5mL 1.7M	1.5mL 2.4M	I pH ~2.0 1M HCl	180 µL 0.03M	
Np- (400pppm)	1.5mL 1.7M	1.5mL 2.4M	I pH ~2.0 1M HCl		70 µL 0.03M
Np- (1000 ppm)	1.5mL 1.7M	1.5mL 2.4M	I pH ~2.0 1M HCl		180 µL 0.03M

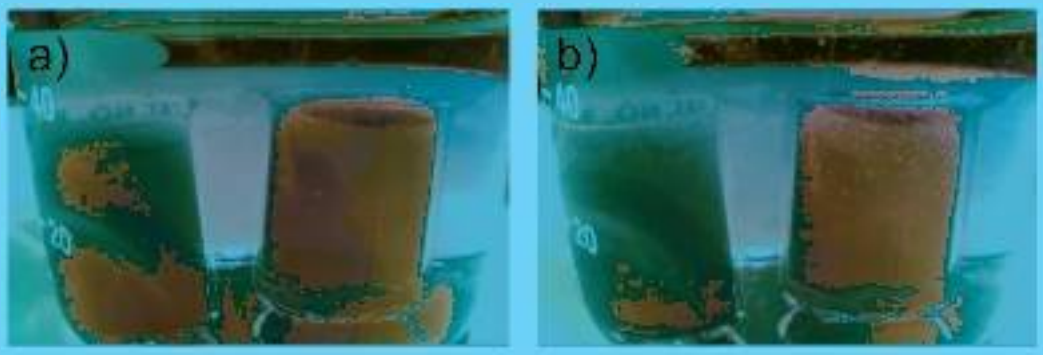

Fig. S1. Photograph of the apparatus for synthesis of calcite crystals from aqueous solution. The photos above, labeled a) and b), are for a synthesis experiment in which the concentrated solutions of $CaCl_2$ and $(NH_4)_2CO_3$ in the vials were dyed purple and yellow, respectively, for 510 min and calcite crystals were apparent at the base of the 2-mL vial. The vial was initially loaded with $(NH_4)_2CO_3$ (aq) and after 1,680 min shows abundant calcite crystals on both vials. The strong colouration of the solution in the 2-mL vials demonstrates that complete solution mixing has not occurred in the system.

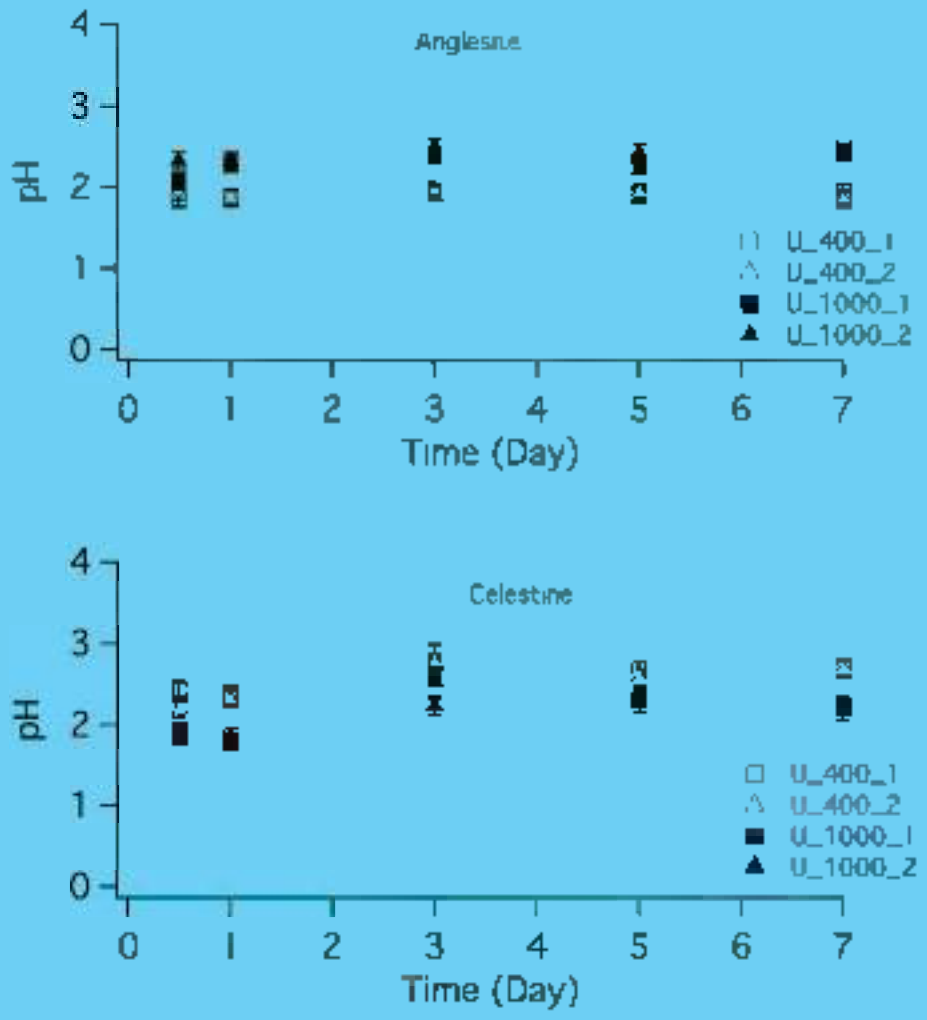

Figure S12 Measured pH of the aqueous buffered solution in anglesite (top) and celestine (bottom) systems. The synthesis experiments began using the apparatus shown in Figure 1 with a starter solution at pH = 2

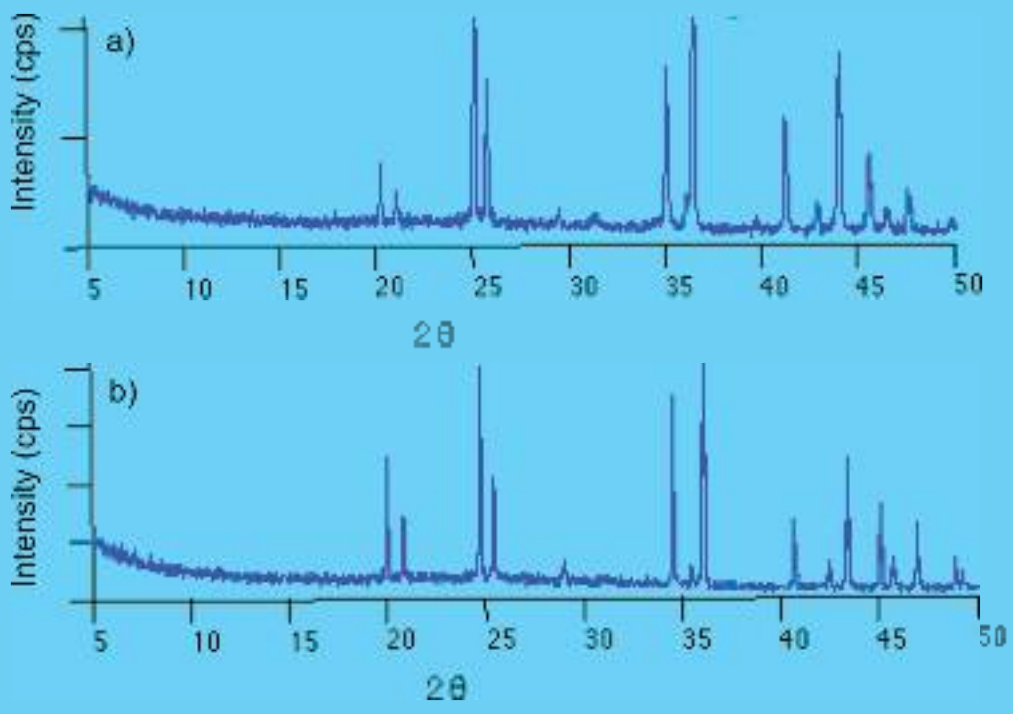

Figure S1. Powder diffraction patterns collected by Cu Kα radiation at ambient temperature and pressure. No additional peaks beyond those characteristic of the two mineral phases were observed. PDF files to which these two powder patterns were compared are 01-084-1778 (strontianite) and 00-047-1417 (witherite).

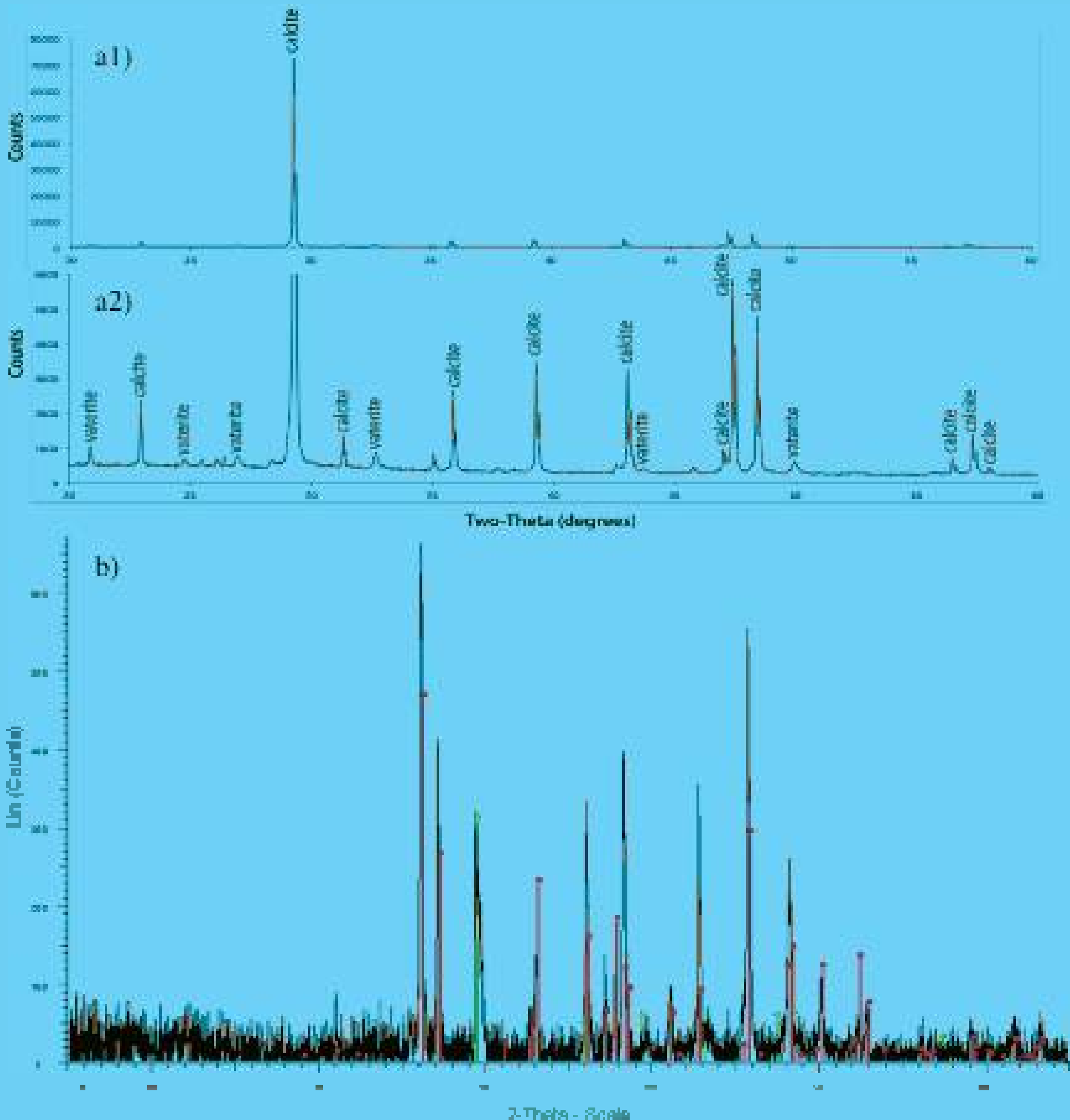

Figure S14. a1) X-ray powder pattern [illegible] radiation for crystals of harvested [illegible] a2) Peaks arising from calcite and vaterite are labeled. [illegible] scales are used so that the full intensity of the calcite peaks are visible. b) Powder pattern of synthetic aragonite (in black) [illegible] the reference aragonite PDF file 01-076-0606 (red in picture). One peak at [illegible] 2θ corresponds to a calcite peak (PDF 01-086-2334 in green).

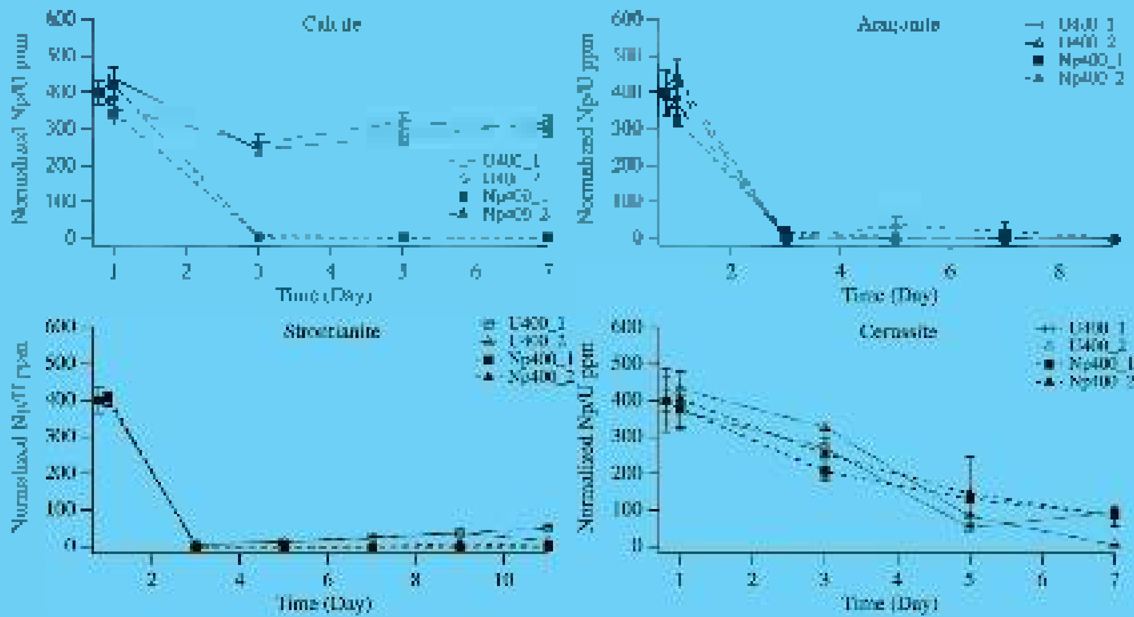

Figure S15. ICP-MS results for the filtered solutions in the synthesis of all carbonate minerals showing actinide concentration in ppm versus reaction time. Data displayed for low concentration experiments (400 ppm).

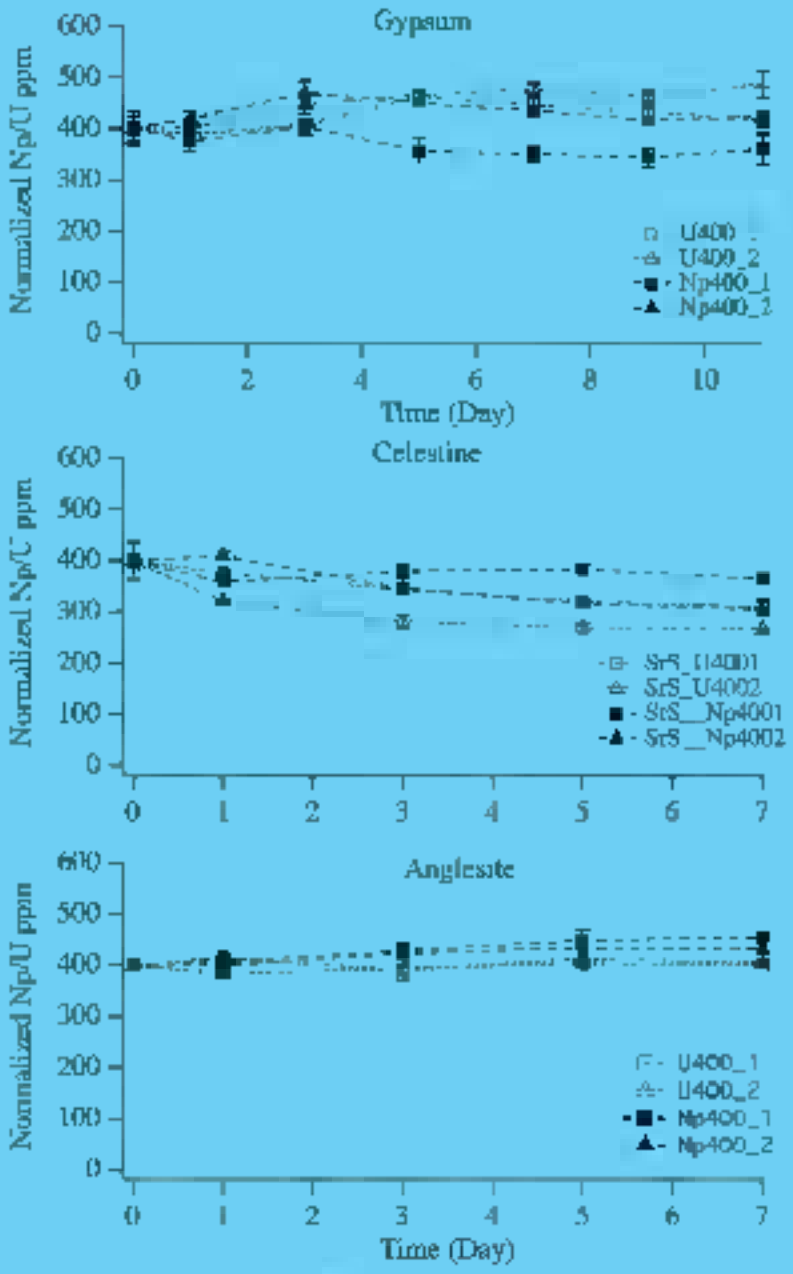

Fig. S1 ICP-MS results for the binary solutions at the saturation of all solubility minerals showing actinide concentration (in ppm) versus reaction time. Data displayed for low concentration experiments (400 ppm).

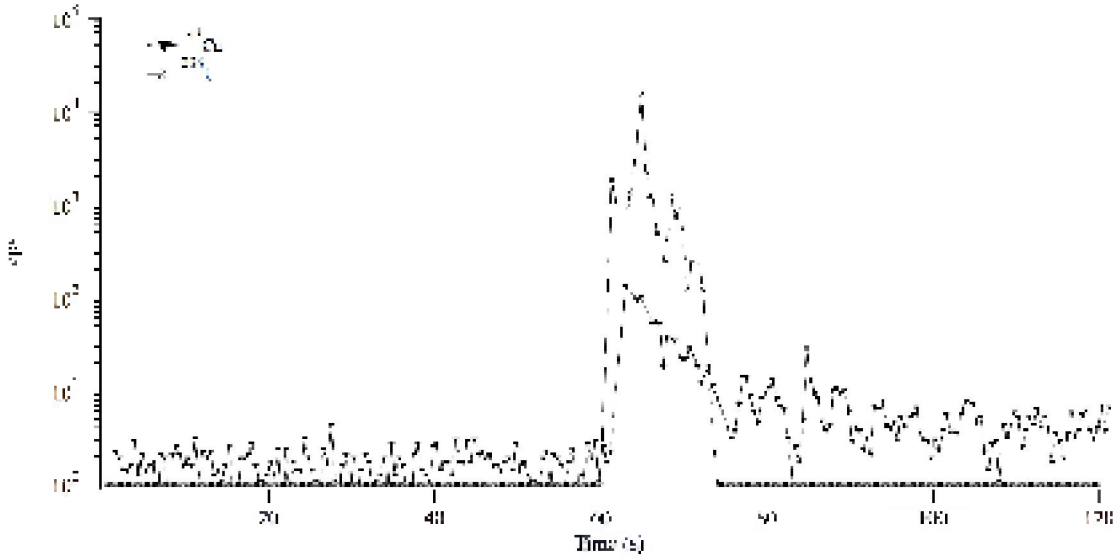

Figure SI 7 Laser ablation pattern of a crystal of gypsum crystallized from a 1000 ppm U solution. The laser strikes at 60 seconds and both ^{238}U and ^{43}Ca counts spike in intensity, indicating that the laser is ablating the material. After about 10 seconds of ablation the ^{43}Ca counts settle to an average value of ~ 3000 cps higher than the background measured between 0 and 60 seconds. The uranium counts, although initially high, decline rapidly during ablation. . This ablation behavior indicates that most of the uranium is present on or near the surface of the mineral.

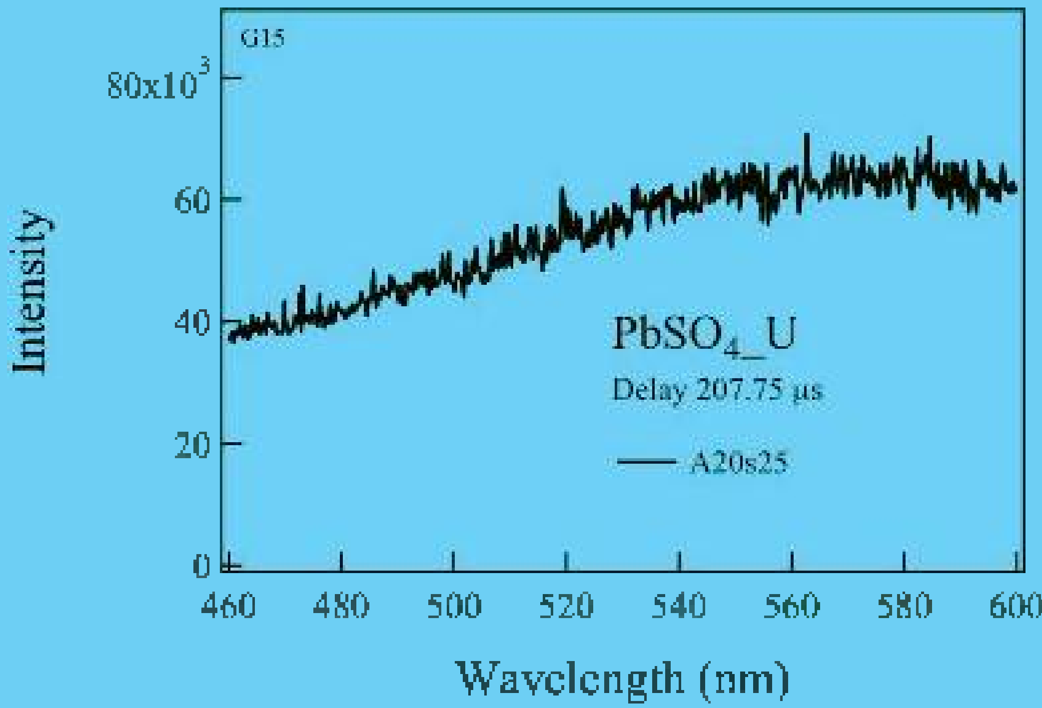

Figure S18 Luminescence spectra of anglesite collected at cryogenic He temperature of 10 ± 1K

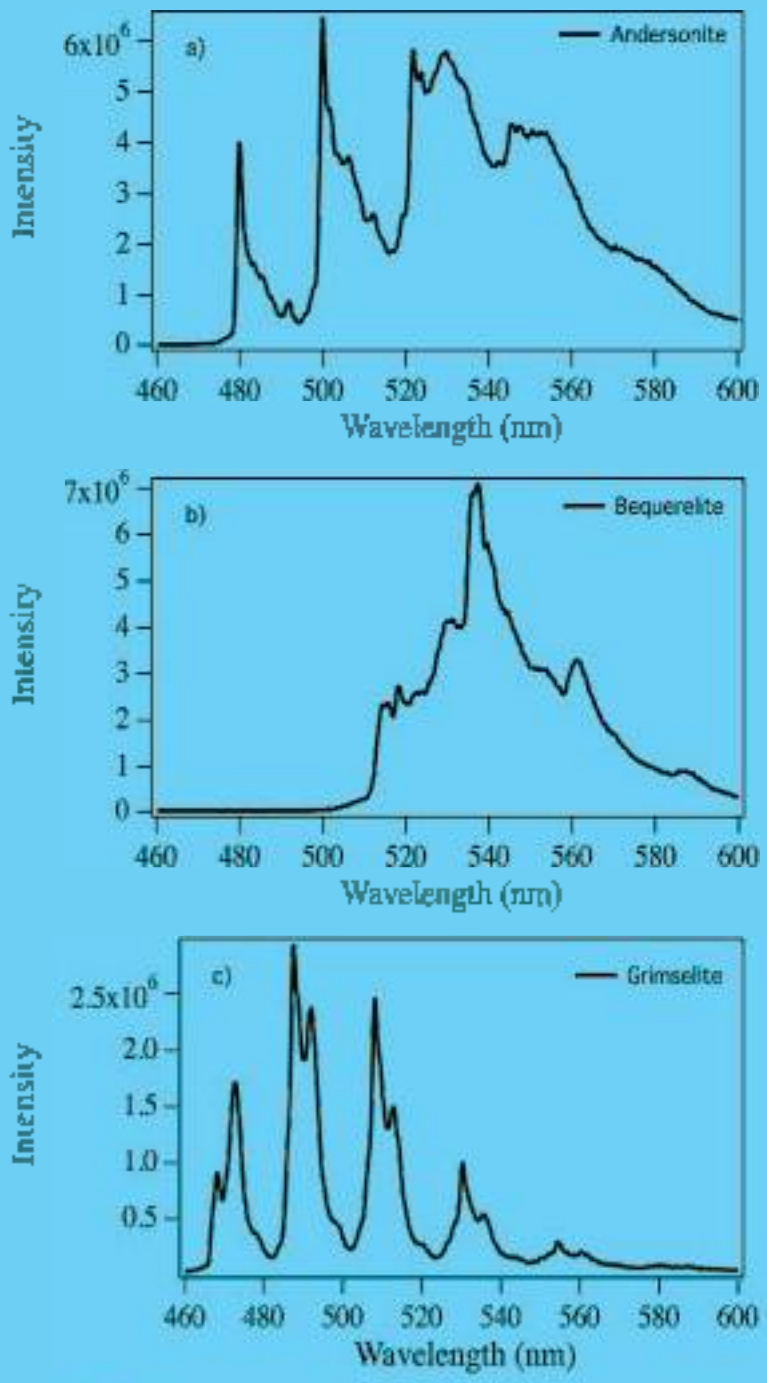

Figure S19. Luminescence spectra of synthetic uranyl minerals andersonite $Na_2Ca[UO_2(CO_3)_3]\cdot 6H_2O$, becquerelite $Ca[UO_2]_6O_4(OH)_6\cdot 11H_2O$, and grimselite $K_3Na[UO_2]_4O_3(CO_3)_4\cdot 1.5H_2O$ collected at cryogenic temperature of 10 ± 1K.

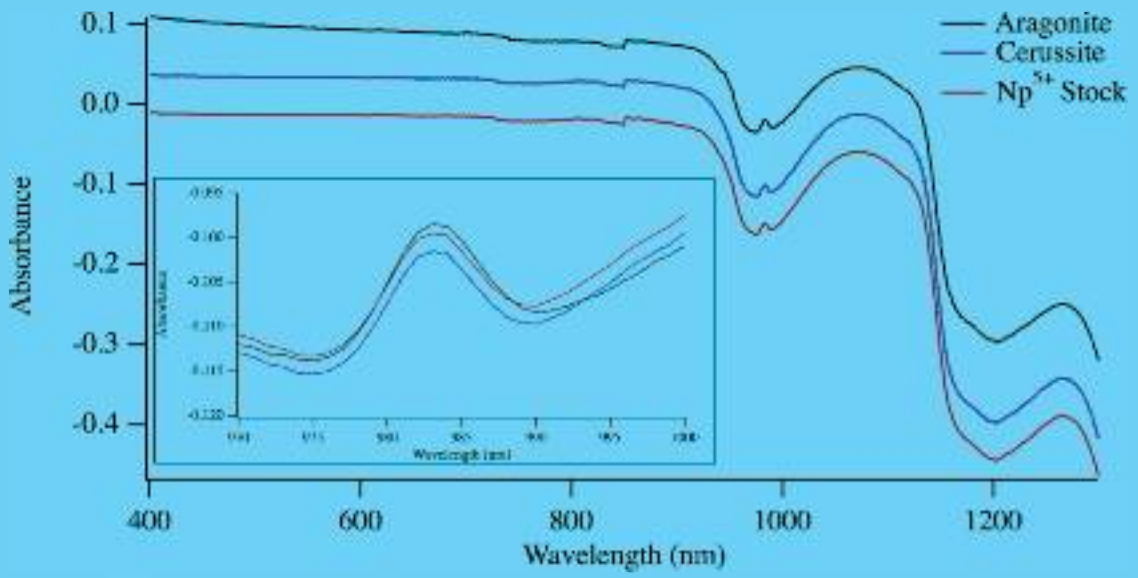

Figure S1. UV-Vis spectra of dissolved precipitates of aragonite (black) and cerussite (blue) 70 mg of material were dissolved in 1M HCl for each mineral phase. The spectra displays the 980 nm peak typical of pentavalent neptunium and is compared to the UV-vis spectra of a Np^{5+} stock solution (red). The inset in the figure represents detail of the 980 nm peak.

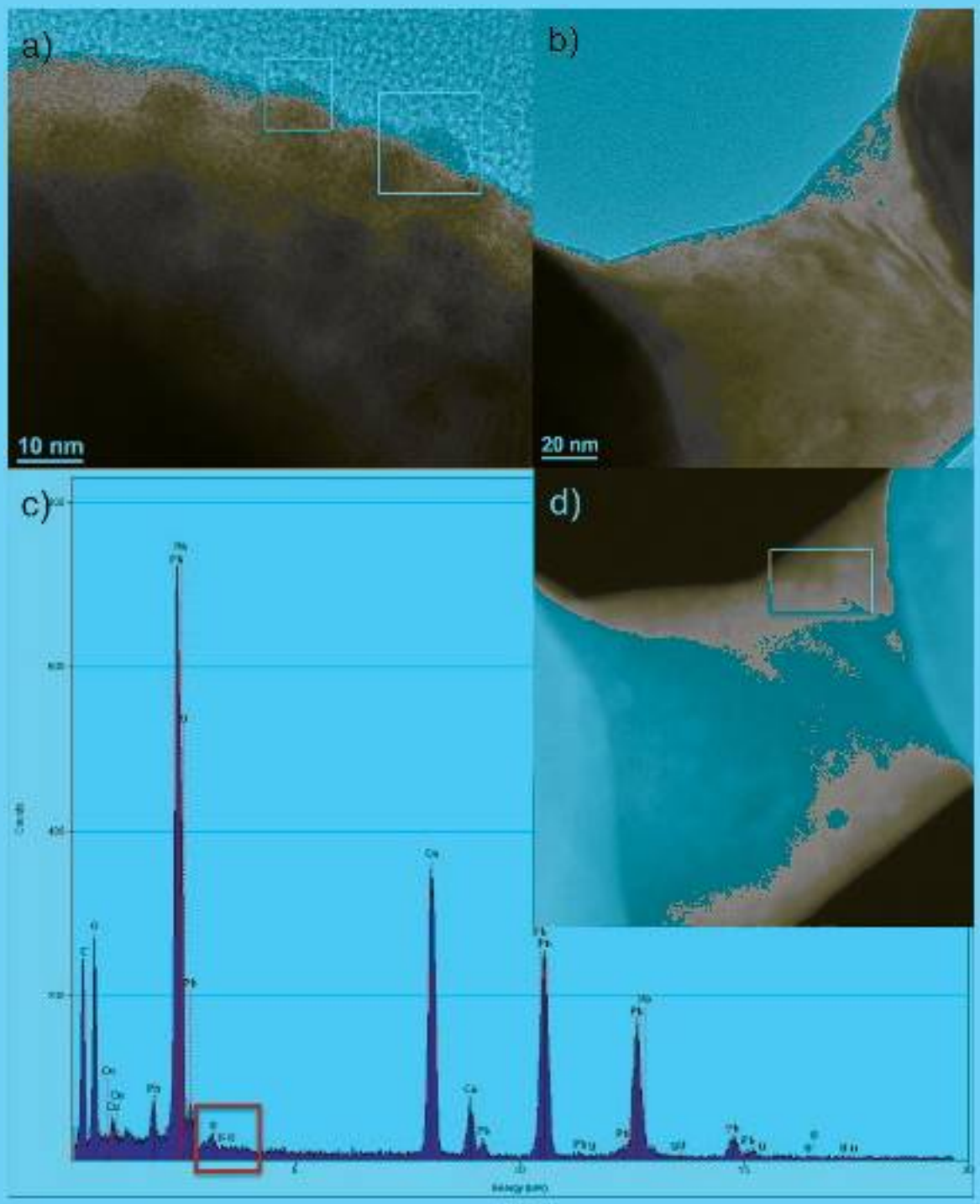

Fig. S1. High resolution TEM of cerussite exposed to U-bearing solutions (pH 6). The white boxes in a) and c) are the areas in which d-spacing was calculated. STEM imaging for and EDS analyses (d) of U-bearing precipitates revealed with the cerussite in the surface (b, c). The white box in b) the point where EDS was performed. The red line in red, shows the presence of uranium.

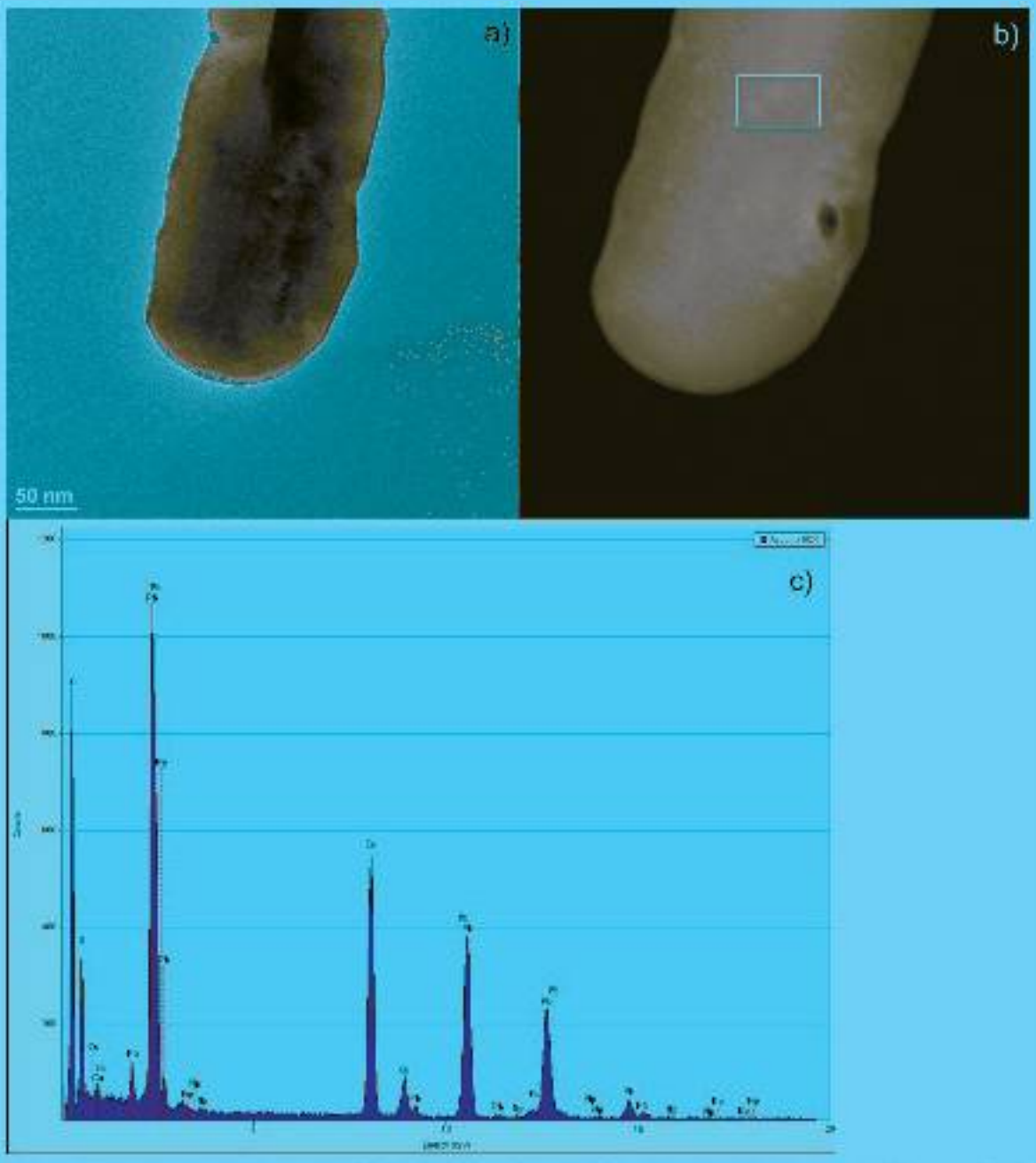

Figure S1 – High resolution TEM (a), STEM (b) and EDS (c) imaging of nepheline precipitate associated with the cementitious matrix. The white box in b) is the location where EDS was performed. The inset shows the presence of uranium. The EDS spectrum is shown in c).